Aerospace Engineering Department
Middle East Technical University

METU-PHOENIX
Let's Re-Engine the Concorde!
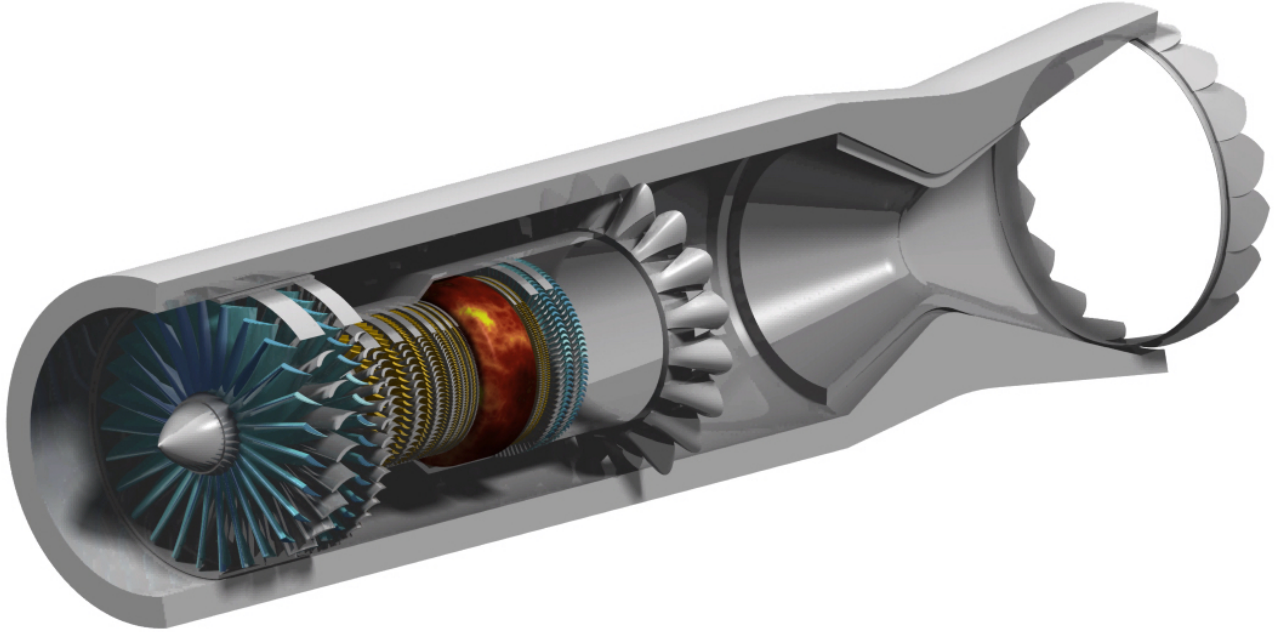
Team Leader

Berkay Keleş

Team Members

Mohamed A.K.I Ahmad
Duygu Çetin
Abdessamad Idoumghar
Ali Mohaghegh
Irem Yılmaz
Cansın Yollar

Faculty Advisor

Asst.Prof. Sıtkı Uslu

MIDDLE EAST TECHNICAL UNIVERSITY

Signatures

Faculty Advisor
Asst. Prof. Sıtkı Uslu
Middle East Technical University
Aerospace Engineering Department
AIAA Member Number : 506268

Team Leader
Berkay Keleş
Middle East Technical University
Aerospace Engineering Department
AIAA Member Number : 1109546

Team Member
Mohamed A.K.I Ahmed
Middle East Technical University
Aerospace Engineering Department
AIAA Member Number : 1241016

Team Member
Duygu Çetin
Middle East Technical University
Aerospace Engineering Department
AIAA Member Number : 1230944

Team Member
Abdessamad Idoumghar
Middle East Technical University
Aerospace Engineering Department
AIAA Member Number : 1241028

Team Member
Ali Mohaghegh
Middle East Technical University
Aerospace Engineering Department
AIAA Member Number : 834083

Team Member
Irem Yılmaz
Middle East Technical University
Aerospace Engineering Department
AIAA Member Number : 1241017

Team Member
Cansın Yollar
Middle East Technical University
Aerospace Engineering Department
AIAA Member Number : 1230935

ABSTRACT

The METU PHOENIX engine is a two-spool, mixed flow, low-medium bypass ratio turbofan engine developed for the Concorde, a supersonic jet. The METU PHOENIX engine has the ability of supersonic cruise at Mach 2.0. As lighter weight, lower take-off noise, lower emissions at high altitudes, and lower fares are desired, the METU PHOENIX is intended to meet the general changes specified in the Request for Proposal. Furthermore, all along the design point and off-design engine missions, minimizing the rate of overall fuel consumption, noise, dry weight and maximizing performance is well-considered for the best operating performance.

Table 1: METU-PHOENIX Engine Technology Features

Engine Component	Description
Inlet	2 Ramp Mixed Compression Supersonic Inlet made of CFRP
Fan	2 Stage Fan High Efficiency with Polyimide Blades
High-Pressure Compressor	7 Stage of HPC manufactured with Titanium Superalloy Blisk
Combustion System	Lean Direct Injection Combustor with Hybrid Diffuser
High-Pressure Turbine	2 Stage of cooled HPT manufactured from CMC
Low-Pressure Turbine	2 Stage of uncooled LPT manufactured from CMC
Mixer	Force Flow Lobed Mixer with Chevrons
Exhaust System	Fully Variable Con-Di Nozzle Made Out of Noise Absorbing Material

Table 2: METU-PHOENIX Engine Feature

	Olympus 593	METU PHOENIX	Engine Feature Comparison Percent Difference [%]
Dry Weight [kg]	3175	1680	-47
Length [m]	4.039	6.0	+49
Max. Fan Diameter [m]	1.3	1.4	+7

iv

Contents

List of Figures

List of Tables

INTRODUCTION

AIAA undergraduate team gas turbine engine design competition 2020/21 "Let's Re-Engine the Concorde !" is about preliminary design of supersonic turbofan engine suitable for Concorde. The METU PHOENIX engine is a candidate engine for the Concorde, a supersonic jet engine capable of replacing the baseline turbojet engine i.e. Olympus 593. Table 3, 4 represent the general characteristics of the Concorde aircraft and its engine Olympus 593 respectively which has been obtained from the Request for Proposal (RFP) [11].

Table 3: General Specifications of Concorde Aircraft

Parameter	Value
Crew	3
Capacity	92-120
Height [m]	8.5
Length [m]	61.7
Wing Area [m^2]	358.3
Wingspan [m]	25.6
Power Plant	4 ×Rolls-Royce/Snecma Olympus 593 Mk 610 Turbojet
Maximum Take-off Weight [kg]	18,570
Maximum Mach Number	2
Cruise speed [m/s]	590
Range [km]	7223
Service Ceiling [km]	18.3

It is specified in RFP that the current inlet will be retained. Also in RFP, T3 and T4 are limited to 900 K and 1720 K, respectively. In addition, it is specified in RFP that the jet velocity at take-off should not exceed 350 m/s due to noise restrictions. This information and Table 3 is taken into account in performance calculations. In addition, Table 4 lists the design features of the baseline engine defined in the RFP. Although these features are tabulated based on the RFP, they will be updated and improved in the following sections in order to meet the mission requirements. Table 4 shows the baseline engine Olympus 593.

Table 4: Olympus 593 Engine Specifications

Parameter	Description/Value
Engine Type	Turbojet
Number of Compressor stage	7
Number of HP/LP Turbine stages	1 , 1
Combustor Type	Annular
Maximum Net Thrust at Sea Level [kN]	169.2
Specific Fuel Consumption at Max. Power[g/(kN*s)]	33.71
Overall Pressure Ratio at Max. Power	15.50:1
Max. Envelope Diameter [mm]	1212
Max. Envelope Length [mm]	4039
Dry Weight Less Tail-Pipe [kg]	3175

The cycle analysis and optimization of the METU-PHOENIX engine at design and off-design conditions are demonstrated in the following chapters. The results of the Concorde engine's supersonic cruise performance is compared to the baseline engine and the RFP's specifications. The base engine was rebuilt with SI unit using GasTurb. In addition, a comprehensive engine part design is demonstrated and justified with the use of advanced technology in the design of the METU-PHOENIX engine. Consequently, the installed engine's output is tested using the GasTurb and AxSTREAM software. Furthermore, the exhaust system is designed using the Method of Characteristics and CFD. In addition, a comprehensive structural analysis is provided, including material selection and manufacturing techniques for each component. The investigation of noise reduction technologies and subsystems, such as anti-icing, secondary power, engine control system, fuel, and lubrication system. Finally, constraints, weight and cost analysis is conducted which are written in the later chapters.

1. CYCLE ANALYSIS

The main structure of the METU-PHOENIX engine is explained in this chapter the cycle analysis software used for the construction of the low-medium bypass turbofan. In this chapter, the optimum cycle configuration is presented.

1.1 Advanced Engine Cycle Concepts for METU PHOENIX

The first step towards the optimum cycle design for the METU-PHOENIX engine is to take a number of different, but promising cycling principles into account and to identify what cycle design would provide the optimal combination of efficiency, complexity, technology readiness (TRL) and cost. As shown in Table 1.1, based on the bypass ratio, a turbofan engine can be classified as low, medium, powerful, or ultra-high bypass. Low-Medium bypass technology was used in the METU-PHOENIX engine to minimize the TSFC and reduce the jet noise as much as possible.

Table 1.1: Turbofan Engine Classification

Type of Turbofan Engine	Range of BPR
Low- Bypass	BPR <2
Medium- Bypass	$2 \leq BPR <5$
High- Bypass	$5 \leq BPR<9$
Ultra-High- Bypass	BPR ≥ 9

It is critical to scale the nozzle properly in the preliminary design of the METU-PHOENIX engine to satisfy the RFP specifications; thus, achieving high performance in supersonic cruise and noise reduction to be feasible. Furthermore, for optimal efficiency in supersonic flight, a fully variable converging-diverging (Con-Di) nozzle with noise absorbing material is designed with considering both on-design and off-design performance specifications that must be met with low noise levels.

1.2 Engine Components and Diagrams

The METU-PHOENIX engine is designed as a low-medium bypass, mixed flow axial turbofan engine with two spools. The engine consists of air intake system, 2 stage fan, 7 stage high-pressure compressor (HPC), combustion chamber and fuel atomization system, 2 stage of high pressure turbine (HPT), 2 stage of low pressure turbine (LPT), mixer and exhaust system. Engine auxiliary systems, such as the lubrication system, anti-icing system, auxiliary power unit (APU), and starting system, are thoroughly taken into consideration in addition to these main systems and components. Furthermore, the METU-PHOENIX engine performs better compared to the low bypass ratio engines available in the market. The reason behind this superiority can be explained by having better cruise capabilities and reducing fuel consumption tremendously by eliminating the afterburner. Considering main issues that Concorde aircraft has experienced in the history; team paid a special attention to the reduction of noise level and weight of the engine.
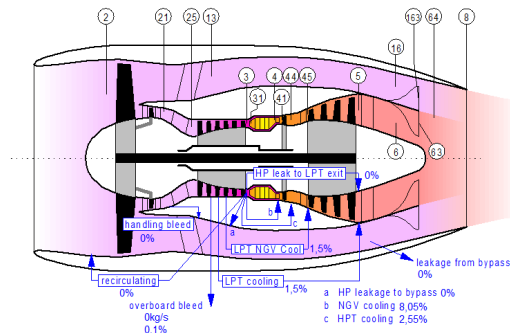
Figure 1.1: Station Numbers for the METU PHOENIX Engine

1.3 Baseline Engine Cycle Analysis and Validation

This part of the preliminary design briefly explains the on-design and off-design performance review and validation of the baseline engine replicated with GasTurb 13 from the RFP.

1.3.1 On-Design Analysis of Baseline Engine: Simulation Validation

According to the RFP, the baseline engine's design point requires a necessary cruise thrust of 44.62 kN at ISA +5. Figure 1.2 shows the baseline engine performance characteristics at cruise condition. The gas turbine engine simulation software GasTurb 13 is used to verify the specific cycle parameters supplied by the RFP for the cruise condition using the SI unit.

```
              W           T          P        WRstd
Station    kg/s          K         kPa        kg/s              FN       =      44.62 kN
amb                   216.64     10.039                         TSFC     =    36.4179 g/(kN*s)
   1      131.245    389.88      78.614                         FN/W2    =     340.01 m/s
   2      131.245    389.88      73.661     209.997             WF Burner=    1.62512 kg/s
  24      131.245    610.29     302.011
  25      131.245    610.29     298.991      64.729             P2/P1    =      0.9370
   3      127.307    854.31     867.075      25.616             P25/P24  =      0.9900
  31      112.879    854.31     867.075                         P3/P2    =     11.7711
   4      114.504   1350.00     832.392      30.169             P45/P44  =      0.9800
  41      121.066   1324.60     832.392      31.597             P6/P5    =      0.9800
  43      121.066   1086.16     323.315
  44      127.629   1074.66     323.315
  45      127.629   1074.66     316.848      78.820             W_NGV/W25=    0.05000
  49      127.629    870.80     122.049                         WHcl/W25 =    0.05000
   5      131.566    867.51     122.049     189.520             WLcl/W25 =    0.03000
   6      131.566    867.51     119.608                         XM6      =    0.25000
   8      131.566    867.51     119.608     193.388             A8       =    0.84651 m²
Bleed      1.304     854.31     867.074                         WBld/W2  =    0.00993
-------------------------------------------------              Ang8      =      20.00 °
Efficiencies:    isentr  polytr    RNI     P/P               CD8       =    0.96000
 LP Compressor   0.8530  0.8782  0.507    4.100              P8/Pamb   =   11.91458
 HP Compressor   0.8170  0.8402  1.208    2.900              WlkLP/W25=    0.00000
 Burner          0.9900                   0.960              Loading  =     100.00 %
 HP Turbine      0.8900  0.8782  1.379    2.575              e444 th  =    0.85894
 LP Turbine      0.9000  0.8885  0.666    2.596              WlkO/W25 =    0.00000
-------------------------------------------------
HP Spool mech Eff 0.9900 Nom Spd      8382 rpm               PWX       =       74.6 kW
LP Spool mech Eff 0.9900 Nom Spd      5819 rpm               Core Eff =     0.5302
-------------------------------------------------            Prop Eff =     0.7776
Con-Di Nozzle:                                               A9/A8     =    1.80000
 A9*(Ps9-Pamb)              5.871                            CFGid     =    0.97386
-------------------------------------------------
hum [%]    war0       FHV      Fuel
   0.0   0.00000    43.124    Generic
```

Figure 1.2: Validation of Olympus 593 Baseline Engine Output Summary at Cruise in SI unit

1.3.2 Off-Design Analysis of Baseline Engine: Simulation Validation

The Concorde is assumed to take off at ISA +10 and standard sea level conditions, as specified in the RFP. Since the required cruising altitude is 16154 m (53,000 ft) , and flight with Mach number 2.0 is expected, the engine must be capable of supersonic cruise at this altitude. Off-design analysis for the baseline engine is performed with GasTurb 13's "Mission" section. The altitude is maintained constant for flight observation in main parameters including specific fuel consumption (TSFC), overall pressure ratio (OPR), turbine entry temperature (TET) and (T_3) in order to produce the required thrust at take-off design point and specified Mach numbers.

Table 1.2: Cruise and Take-Off Conditions Comparison of Baseline Engine

	Cruise	Take-off
Mach	2.0	0.30
F_n [kN]	44.62	149.51
TSFC [g/(kN s)]	36.42	18.58
TET [K]	1350	1352
OPR	11.77	15.97

1.4 METU PHOENIX Cycle Analysis : New Engine Optimization

The following procedure is used in the preliminary design of the METU PHOENIX engine, after the parametric cycle review of the baseline engine by the GasTurb 13. Instead of takeoff, the design point for an engine with supersonic flight capability should be considered top-of-climb, or the starting of the cruise. Furthermore, as stated in the RFP, the METU PHOENIX engine achieves supersonic cruise at Mach 2 at 16154 m altitude, where the design point criterion is validated. The METU PHOENIX engine's design point optimization aims to reduce specific fuel consumption and off-design point optimization aims to reduce the noise in the flight envelope. In addition, in order to reduce the weight of the engine, the METU PHOENIX engine is developed to take into account of the promising technological developments using advanced materials and production techniques. The maximum inlet temperature of the turbine, indicated in RFP as 1750 K, is another significant design constraint. Since it is known that NOx emission is proportional to TET, the upper limit for the TET is held at 1720 K to avoid exceeding NOx emission requirements. According to research [?], by using ceramic-matrix-composite (CMC) materials resistant to temperatures up to 1850 K, turbine inlet temperature limitation can be overcome without using any cooling system, but this has disadvantages such as increasing TSFC and cost [12].

The following section explains how to reduce the METU PHOENIX engine's specific fuel consumption by using the GasTurb 13's "Optimization" section to find the best combination of the four main configuration parameters, bypass ratio, fan pressure ratio, TET, and overall pressure ratio, to meet the desired constraints and satisfy the needed thrust.

1.4.1 On-Design Analysis of METU PHOENIX: Simulation Validation

"Top-of-climb," specified as Mach 2.0 and 16154 m, is the on-design state for a supersonic aircraft. Engines with supersonic capabilities are typically designed for "top-of-climb" conditions rather than take-off, and the METU PHOENIX engine is designed by following this condition. A few restrictions and assumptions were established to begin the analysis.

The effect of the bypass ratio, fan pressure ratio, HPC pressure ratio, and burner exit temperature on TSFC is then addressed using the simulation techniques included in GasTurb 13. Figure below shows some of the most important trade studies for determining the optimum parameters for the METU PHOENIX engine's on-design state. The black dot in figures below carpet plots shows the outcome of the overall optimization.
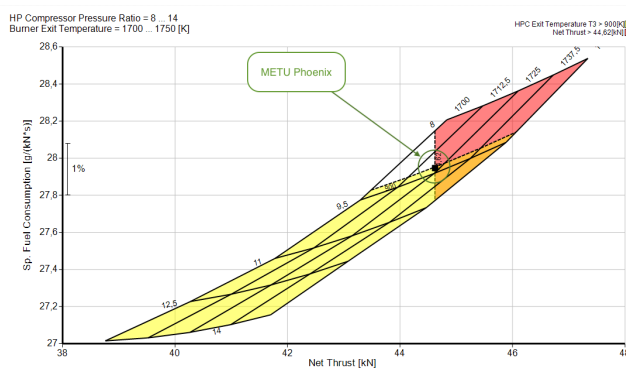
TSFC vs Net Thrust for HP Compressor Ratio vs TET
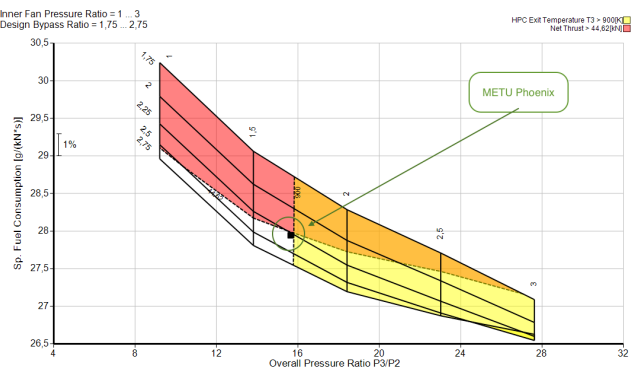
TSFC vs Overall Pressure Ratio for FPR vs BPR
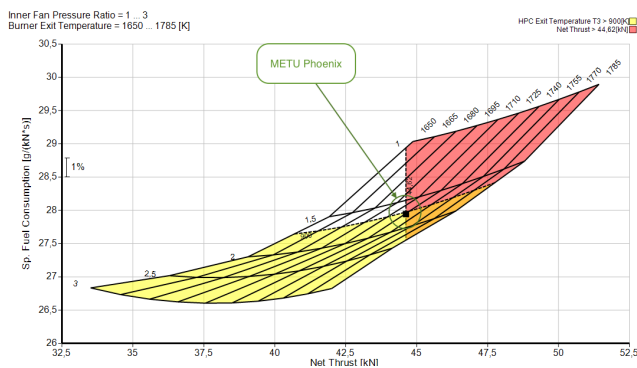
TSFC vs Net Thrust for FPR vs BPR
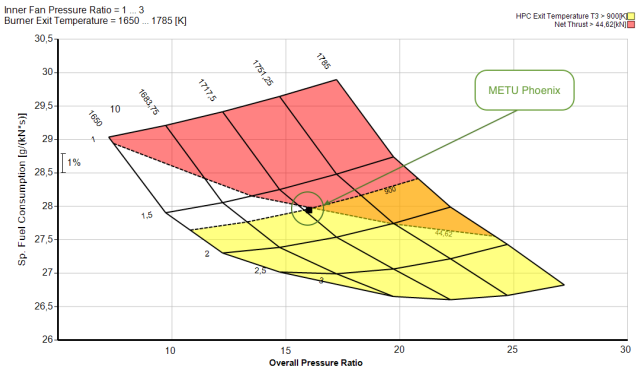
TSFC vs Overall Pressure Ratio for FPR vs TET

Parametric Studies of Cruise TSFC, OPR, BPR, TET and FPR for the METU PHOENIX

The chosen design parameters achieve high stability and efficiency, according to the results of parametric studies. Figure 1.5 shows the METU PHOENIX engine's optimized output at supersonic cruise conditions.

Station	W kg/s	T K	P kPa	WRstd kg/s			
amb		221.65	10.040		FN	=	44.62 kN
1	185.785	398.83	78.612				
2	185.785	398.83	75.074	295.000	TSFC	=	27.9471 g/(kN*s)
13	128.426	477.58	135.134	123.971	WF Burner=		1.24705 kg/s
21	57.359	469.74	127.626	58.143	s NOX	=	1.1347
25	57.359	469.74	126.350	58.730	BPR	=	2.2390
3	55.581	899.92	1175.055	8.470	Core Eff	=	0.6394
31	49.501	899.80	1175.055		Prop Eff	=	0.8357
4	50.748	1721.45	1128.053	11.141	P3/P2	=	15.652
40	52.210	1700.35	1128.053				
41	55.365	1658.17	1128.053	11.930	NGV	2 Stage HPT	
43	55.365	1288.67	324.366		P16/P6	=	0.99037
44	56.828	1279.25	324.366		A63	=	0.57728 m²
45	57.688	1268.49	317.879	38.581	A163	=	0.89370 m²
49	57.688	1061.13	136.448		A64	=	1.47098 m²
5	58.548	1053.35	136.448	83.127	XM63	=	0.40221
6	58.548	1053.35	133.719		XM163	=	0.37382
16	128.426	477.63	132.431		XM64	=	0.40000
64	186.975	669.57	130.855		P63/P6	=	0.99000
8	186.975	669.57	130.855	220.698	P163/P16	=	0.99000
Bleed	0.057	474.25	130.276		A8	=	0.96996 m²

Efficiencies:	isentr	polytr	RNI	P/P	CD8	=	0.95000
					Ang8	=	25.00 °
Outer LPC	0.9105	0.9175	0.503	1.800	P8/Pamb	=	13.03332
Inner LPC	0.9053	0.9120	0.503	1.700	WLkBy/W25=		0.00000
HP Compressor	0.8995	0.9239	0.696	9.300	WCHN/W25	=	0.08050
Burner	0.9995			0.960	WCHR/W25	=	0.02550
HP Turbine	0.9000	0.8861	1.443	3.478	Loading	=	100.00 %
LP Turbine	0.9000	0.8904	0.553	2.330	WCLN/W25	=	0.01500
Mixer	0.6000				WCLR/W25	=	0.01500

WBHD/W21 = 0.00000

HP Spool mech Eff 0.9986 Nom Spd 8818 rpm   far7   = 0.00671
LP Spool mech Eff 0.9986 Nom Spd 4882 rpm   WBLD/W25 = 0.00100
                                               PWX   =   74.6 kW
P2/P1= 0.9550 P25/P21=0.9900 P45/P44= 0.9800   P16/P13 = 0.9800
Con-Di Nozzle: P6/P5   = 0.9800
 A9*(Ps9-Pamb)   4.470   A9/A8   = 2.00000
dT13 Core   =   0.05 dT3 Core   =   -0.12   CFGid   = 0.98796

Figure 1.5: METU PHOENIX Engine Performance at Supersonic Cruise

1.4.2 Off-Design Analysis of METU PHOENIX : Simulation Validation

After determining the cycle parameters for supersonic cruise at the on-design point, it is essential to evaluate the METU PHOENIX engine's performance under significant off-design conditions. According to the RFP, the Concorde takes off at ISA +10 at sea level on a normal day (i.e., a hot day) and fly supersonic at 16154 m with Mach 2.0. A set of mission points corresponding to the above-listed flight conditions were specified in GasTurb 13 to perform the off-design analysis. The goal for the METU-PHOENIX engine's off-design conditions is to achieve the necessary thrust while improving fuel efficiency over the baseline engine. Having the low-medium bypass ratio 2.25 technology and fully-variable nozzle in the METU PHOENIX engine, combining higher thrust with lower TSFC was accomplished at off-design conditions. Also, the noise of the jet engine, has been reduced at take off as specified in RFP. This is achieved by increasing bypass ratio while decreasing exit velocity. Also, fully variable nozzle with chevron was used for METU PHOENIX engine. Only the convergent part is used during take-off so the noise of the engine is reduced so that the exit Mach number is kept at maximum 1. Table 1.3 summarizes the main parameters of the METU-PHOENIX engine's off-design mission.

Table 1.3: Key Parameters of the METU-PHOENIX for all design missions

	Take-off	Cruise
Mach Number	0	2
Altitude [m]	0	16154
Thrust [kN]	149.88	44.62
TSFC [g/(kN s)]	18.6	27.9
TET [K]	1669	1721
OPR	23.61	15.65
FPR	2.37	1.80
BPR	1.87	2.24

Following figure shows the output page of GasTurb for the METU PHOENIX engine at take off condition.

```
              W          T          P        WRstd
Station    kg/s         K         kPa        kg/s           FN        =      149.88 kN
 amb                 298.15    101.325
   1      357.123    303.58    107.941                      TSFC      =      18.5821 g/(kN*s)
   2      357.123    303.58    103.083      360.307         WF Burner=     2.78505 kg/s
  13      232.611    398.80    244.707      113.310         s NOX     =       0.9588
  21      124.513    391.04    227.004       64.743         BPR       =       1.8682
  25      124.513    391.04    224.190       65.556         Core Eff  =       0.4499
   3      120.653    810.53   2433.701        8.425         Prop Eff  =       0.3346
  31      107.454    810.44   2433.701                      P3/P2     =      23.609
   4      110.239   1669.29   2361.461       11.385         P5/P2     =       2.5466 EPR
  41      117.088   1623.31   2361.461       11.924         P16/P6    =       0.93931
  43      117.088   1260.31    678.045                      A63       =       0.57728 m²
  44      123.438   1238.75    678.045                      A163      =       0.89370 m²
  45      123.438   1238.75    663.866       39.063         A64       =       1.47098 m²
  49      123.438   1015.18    262.512                      XM63      =       0.45614
   5      127.173    998.95    262.512       91.395         XM163     =       0.33368
   6      127.173    998.95    256.165                      XM64      =       0.39987
  16      232.611    398.85    240.619                      P63/P6    =       0.98781
  64      359.784    624.04    242.835                      P163/P16  =       0.99170
   8      359.784    624.04    242.835      220.924         A8        =       0.96996 m²
Bleed      0.125     395.42    231.868                      CD8       =       0.95000
-------------------------------------------              Ang8      =       25.00 °
Efficiencies:   isentr  polytr     RNI     P/P             P8/Pamb   =       2.39659
  Outer LPC     0.8899  0.9023   0.956   2.374             WLkBy/W25=       0.00000
  Inner LPC     0.8749  0.8879   0.956   2.202             WCHN/W25 =       0.05500
  HP Compressor 0.8601  0.8965   1.538  10.856             WCHR/W25 =       0.05100
  Burner        0.9997                   0.970             Loading   =      78.85 %
  HP Turbine    0.9013  0.8875   3.095   3.483             WCLN/W25 =       0.00000
  LP Turbine    0.9114  0.9018   1.187   2.529             WCLR/W25 =       0.03000
  Mixer         0.6000                                     WBHD/W21 =       0.00000
-------------------------------------------              far7      =       0.00780
HP Spool mech Eff 1.0000  Speed      8818 rpm             WBLD/W25 =       0.00100
LP Spool mech Eff 1.0000  Speed      4839 rpm             PWX       =        74.6 kW
-------------------------------------------              P16/P13   =       0.9833
P2/P1= 0.9550 P25/P21=0.9876 P45/P44= 0.9791              P6/P5     =       0.9758
Con-Di Nozzle:                                            A9/A8     =       1.00000
 A9*(Ps9-Pamb)      25.616                                CFGid     =       1.00000
dT13 Core      =    0.04  dT3 Core    =   -0.09
-------------------------------------------
```

Figure 1.6: METU PHONEIX Performance at Take Off Condition

1.5 Performance Comparison with the Baseline Engine Model

Table 1.4 compares the performance thermodynamic properties of METU-PHOENIX and Olympus 593 at cruise and take off conditions.

Table 1.4: Performance Parameters Comparision of METU-PHOENIX and Olympus 593

	OLYMPUS 593		METU PHOENIX		Performance Parameters Percent Difference [%]	
Mission	Take-Off	Cruise	Take-Off	Cruise	Take-Off	Cruise
Thrust [kN]	149.51	44.62	149.88	44.62	+0.3	0
T3 [K]	739	853	811	900	+9.7	-5.5
T4 [K]	1352	1350	1669	1721	+23.5	+27.5
Exit Velocity [m/s]	N/A	912	456	817	N/A	-10.5
BPR	0	0	1.87	2.24	N/A	N/A
OPR	16	11.77	23.60	15.65	+47.5	+33
SFC [g/(kN*s)]	N/A	37.69	18.58	27.95	N/A	-26
Outer LPC PR	N/A	N/A	2.37	1.8	N/A	N/A
Inner LPC (FPR)	4.67	4.1	2.2	1.7	-52.8	-58.5
HPC PR	3.46	2.9	10.86	9.3	+213.8	+220.7
HPT PR	2.94	2.52	3.48	3.48	+18.5	+38
LPT PR	2.23	2.49	2.53	2.33	+13.4	-6.4
Burner PR	0.965	0.96	0.97	0.96	+0.5	0
A9/A8	1.8	1.05	1	2	-44.4	+90.5
Prop. Efficiency	0.26	0.78	0.34	0.84	+31	+7.4
Core Efficiency	0.33	0.54	0.5	0.64	+51	+18

COMPONENTS DESIGN

2.   INLET

Even though it is mentioned in the RFP that the current inlet is planned to be retained, inlet is a crucial component for a supersonic engine. That is why designer team considered the preliminary design of it.

Purpose of a supersonic inlet is to decelerate the free-stream Mach number to around 0.5 for the entry of fan. It needs to recover the total pressure of the free-stream while doing so. Supersonic flow creates shocks when it coincides with an obstacle along the way. If the obstacle is an inclined surface, created shock will be oblique. Compared to a normal shock, oblique ones decelerate the flow less and cause less total pressure drop.

A supersonic convergent-divergent inlet consists of a convergent part composed of inclined surfaces called ramps a and divergent part. These ramps decelerate the supersonic flow gradually until the throat. Throat is the minimum area part of the inlet where a normal shock occurs. After a normal shock, flow is always subsonic. However, high subsonic Mach number is needed to be decelerated further. Divergent part between the throat and fan face comes into role at this point. A high performance inlet design is the combination of ramp angles and area ratios that gives the desired Mach with the least pressure loss.

2.1   Inlet Types

There are 3 types of supersonic inlets. External compression inlets consist of number of ramps that create oblique shocks hitting a cowl lip to create normal shock at the throat. The advantage of this type is it is simple, short, lightweight and can be designed to be 2D. However, ramps turn the flow away from axial direction, so the combination of cowl and subsonic part stays as an obstacle in front of the flow and create cowl drag. Due to the positioning of the inclined cowl overall height of the inlet is higher compared to the other types with same fan diameter.

Internal compression decelerate the flow by a series of oblique shocks. They generally have 3D designs. Shocks take place at a confined geometry which creates a complicated flow field due to shock-wave boundary layer interaction. However, this type does not generate the extra cowl drag as flow decelerates axial.

Third and final type of supersonic inlet is the mixed compression one. It has both the external ramps to create oblique shocks and a confined part before the throat. This way, cowl drag disadvantage of external type is eliminated and number of required oblique shocks at internal geometry is reduced.

All types of supersonic inlet types suffer at off-design conditions as the shock angles differ with Mach number. Moreover, subsonic flow accelerates in a converging geometry while supersonic decelerates. That is why variable geometry ramps boost the performance of the inlet but adds complication and weight to the system.

2.2   Design Approach

Mixed compression convergent-divergent inlet is chosen as design inlet for METU-PHOENIX engine for the advantages mentioned in previous subsection. Moreover, since the engine is planned to be mounted on the same air frame, overall engine height is quite critical. Dimensions and Mach number at fan face are obtained from performance calculations. Supersonic part of the inlet brings the flow to a certain subsonic Mach number with a known total pressure. Since the flow is subsonic after the throat, divergent cross-section will decelerate the flow further. There will be a pressure loss due to friction as a function of divergent wall angle [4]. Using mass flow parameter formulas, also known as Q curves, throat area is determined with known Mach number and total pressure ratio.

Unlike the subsonic part, there is no straightforward mathematical relations for the supersonic part. The design process is iterative that must satisfy strict conditions, such as, where the shocks strike and maximum allowable dimensions. Number of ramps is proportional to pressure recovery factor (PRF) but also to weight. PRF is

the ratio of total pressure at the fan face to that of free-stream. 2 ramps are observed to give satisfactory PRF. Both the ramps are varied between 1 and 20 degrees with 100 equal spacing which assigns 100 different angle of second ramp for a certain first ramp angle. That makes 10,000 considered combinations. Cowl deflection is equal to the sum of the deflection of 2 ramps. It is simpler to explain the procedure in an example, for the visualization refer to Figure 2.1.
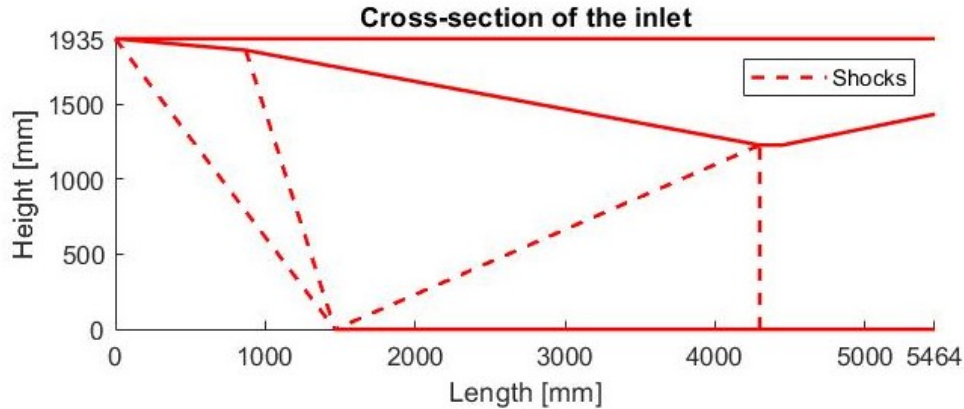
Figure 2.1: Cross-section of the inlet at design point

For example, angle combination is such that the first ramp angle is 3 and the second is 5 degrees. Shock angle and Mach number after the first ramp is calculated with oblique shock relations. This reduced Mach number is deflected once again with the second ramp. One last deflection with 8 degrees takes place before throat due to cowl. Knowing the shock and deflection angles, length and the position of the ramps and the cowl can be calculated using analytical relations such that the shocks hit the shown points at the figure.

All the combinations are considered and configuration that gives highest PRF with desired throat Mach number and satisfying given constraints is registered as design point. It was observed that throat Mach number of 0.8 results in the highest PRF for flight Mach number of 2.

Table 2.1 shows geometric parameters of the optimized supersonic mixed compression convergent-divergent inlet for design point with explained approach. The procedure is formulated in MATLAB.

Table 2.1: 2D design of the inlet

Parameter	Dimensions
First ramp angle (θ_1) [deg.]	5.030
First ramp angle (θ_2) [deg.]	5.222
First ramp length [mm]	859
Second ramp length [mm]	3532
Cowl length [mm]	1494
Throat diameter [mm]	1234
Subsonic wall angle [deg.]	10
Subsonic wall length [mm]	1141
Fan face diameter [mm]	1432
Overall inlet length [mm]	5606
Overall inlet height [mm]	1938
PRF	0.926
M_{throat}	0.800
M_{fan}	0.500

Theoretically, optimum inlet decelerates the free-stream Mach number in a continuous fashion with infinite number of oblique shocks [5]. This way the created shocks have the same strength. Usually in practice, this is not possible. Strength of series of shocks can be visualized by Mach number. An ideal inlet would decelerate Mach 2 to 0.8 in a linear trend. Difference of deceleration between design and optimum inlet is shown at Figure 2.2. Horizontal axis of the figure represents Mach number after a shock. For example, 2 in x-axis is the Mach number after the 1st shock.

9
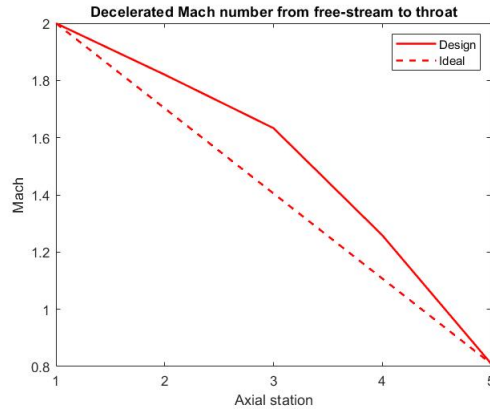
Figure 2.2: Shock strengths

Table 2.2: 2D Inlet CFD Properties

Mesh Program	ICEM CFD	Yplus is below 1 along the nozzle wall	
Mesh Technique	Block Mesh		
Solver		**Boundary Conditions**	
Program	Fluent	**Inlet**	Pressure Far Field Gauge Pressure: 10040 [Pa] Temperature= 217 [K] Mach number = 2
Type	Density-based	**Outlet**	Pressure Far Field Gauge Pressure: 61600 [Pa] Temperature= 377 [K] Mach number = 0.54
Time	Steady	**Inlet**	Wall
2D Space	Planar	**Materials**	
Models		**Fluid**	Air
Energy	on	**Density**	Ideal-gas
Viscous Model	k-omega , SST	**Viscosity**	Sutherland

Figure 2.3: 2D CFD Mach Contour for Inlet

To validate the results that has been obtain from team's MATLAB code, two available comparison are MIL-E-5008B standards and CFD analysis. Standards is formed with historical trends and specific inlet designs. They reflect the general performance of supersonic inlets and for Mach numbers between 1 and 2 the relation is given in Equation 2.1 [5]. Table 2.2 is a summary of the CFD configuration used in the analysis. Comparison of the PRF can be seen at Table 2.3 for cruise.

$$PRF = 1 - 0.075(M_0 - 1)^{1.35} \qquad (2.1)$$

Table 2.3: PRF comparison

-	MIL-E-5008B	2D Shock Relations	CFD Results
PRF	0.925	0.926	0.906

10

2.3 Normal Shock at Throat

Contraction ratio C_r is an important performance parameter in the inlet design. It shows whether a normal shock is going to occur at the throat or not. For an isentropic flow, supersonic area ratio for sonic conditions at throat is shown in Equation 2.2.

$$C_r = \frac{A_\infty}{A_{th}} = \frac{1}{M_\infty} \left[\frac{2}{\gamma+1} \left(1 + \frac{\gamma-1}{2} M_\infty^2 \right) \right]^{\frac{\gamma+1}{2(\gamma-1)}} \tag{2.2}$$

Where A_∞ is the capture, A_{th} is the throat area. For a mixed compression inlet the capture area is replaced with internal capture area which is denoted as A_{cl} [13]. Subscript cl stands for "enclosed area". A_{cl} for the design inlet is the perpendicular distance from cowl tip to the 2nd ramp, see Figure 2.1. Moreover, the Mach number in Equation 2.2 is replaced with the one after 2nd ramp.

If the geometrical contraction ratio is lower than the computed one, normal shock is not going to occur at throat. On the other hand, if it is higher, then, the shock is going to occur before the throat. However, Equation 2.2 is isentropic, many other phenomenons occur in real life. The most common one to explain is viscous effects, for example, subsonic flow through a constant cross-section frictional duct chokes due to total pressure loss. These unaccounted effects result in a different shock location. For this reason a 5% relative error is given as a tolerance between the calculated C_r with Mach number and obtained one with geometry, so that when the obtained geometry is analyzed in advanced simulations, optimization process takes less time.

As it can be seen from Figure 2.3, the shock occurs before the throat which means the C_r is over predicted. However, fan inlet Mach number is around 0.54 looking at the contours, which is quite close compared to the desired 0.5. However, it is already mentioned that a tolerance is given for the contraction ratio. After this point, accurate CFD optimization process should take place and dimensions should be updated. Unfortunately, designer team is lack of the computational power for iterative optimization runs.

2.4 Off-design Operation

Any Mach number other than the design one is going to result in a different shock intensity, i.e. shock angle and upstream Mach number, for a given deflection angle. Since Concorde is a commercial aircraft and its design point is cruise, off-design points are going to be less than 2. These operations are going to result in higher shock angles and spillage will occur if the ramp angles are kept constant. Disadvantage of the spillage is there will be more drag and expected mass flow rate will be reduced.

Designer team have had hard time designing a variable geometry ramp system with a constant overall inlet height. Explained design approach works for smaller Mach number but the optimum point has different overall height other than that of design. Changing the height of the engine would require an extra actuator to lift and lower the cowl plane of the engine. However, one set of solution that the team thought of is, cowl plane can be placed for design overall inlet height and not displaced throughout the flight. Reduction in height of the engine between start of the first ramp and fuselage at lower Mach numbers will result in an empty space. This cavity can be used as bleed air to feed extra mass flow at off-design operations.

Table 2.4: Off-design parameters

Parameters	Flight Mach number				
-	1.5	1.6	1.7	1.8	1.9
First ramp angle [deg.]	1.576	2.343	3.111	3.687	4.263
Second ramp angle [deg.]	1.768	2.343	3.111	3.879	4.646
First ramp length [mm]	188	278	398	528	682
Second ramp length [mm]	2395	2619	2824	3064	3305
Overall inlet length [mm]	3853	4162	4479	4838	5219
Overall inlet height [mm]	1379	1459	1561	1671	1796
PRF	0.943	0.941	0.939	0.936	0.931
M_{fan}	0.500	0.500	0.500	0.500	0.500

(a) Side view

(b) Side view with sectioning

(c) Isometric view

(d) Isometric view with fan
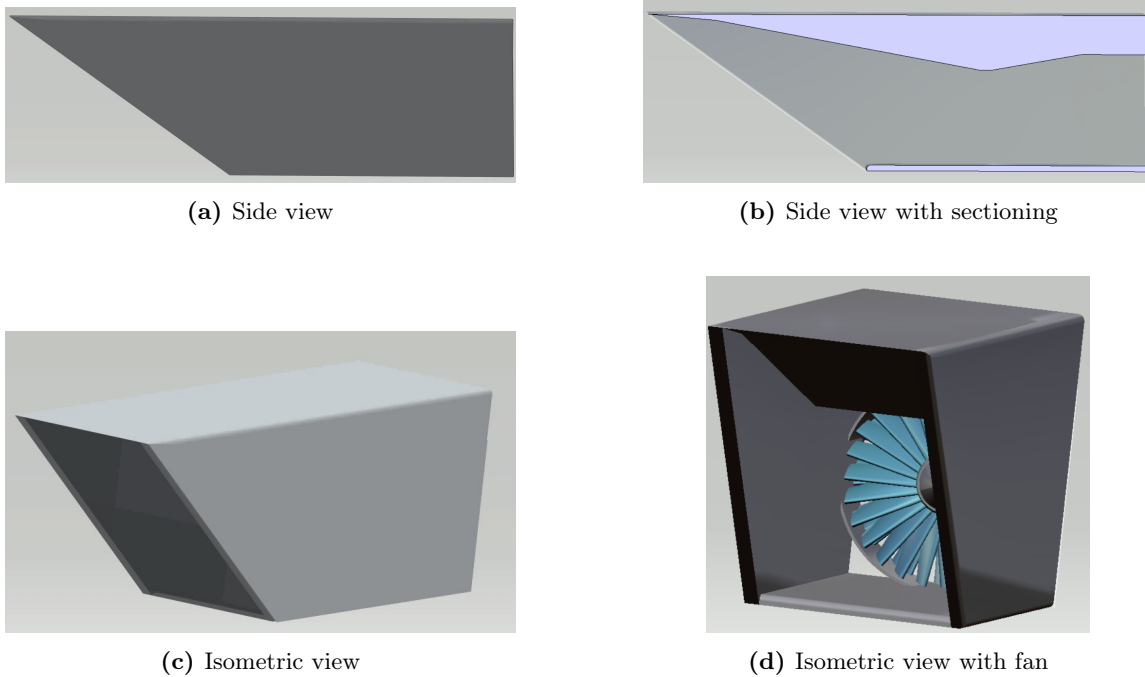
Figure 2.4: CAD drawings of the inlet

Keeping the throat Mach number constant (0.8), there is no need to change the geometry of divergent section. Only the ramp angles and lengths are going to change. Since optimum dimensions are calculated, single actuator is going to be enough for a ramp. A geometrically scheduled actuator just like the ones used in the variable nozzle mechanism could be a way to go option [14]. If such mechanism is designed for the inlet, PRF of around 0.93 can be sustained throughout the flight. Table 2.4 contains a summary of the geometrical parameters of off-design inlet performance. Ramps start moving from their minimum positions at Mach 1.5 until the maximum at Mach 2. If it is desired to have a variable geometry for lower Mach numbers that 1.5, divergent section of the inlet should be variable as well. This configuration of inlet, see Figure 2.1, is not able to produce Mach 0.8 flow at throat for $M_\infty < 1.5$.

2.5   Material and Manufacturing

The inlet experiences temperatures up to 385 K during Mach 2.0 operation. METU-PHOENIX team decided to use Carbon Fiber Reinforced Polymer (CFRP) for the inlet. CFRP materials benefits from high toughness and durability which can lead to great advantages such as low maintenance cost. Moreover, CFRP materials have low density which will result in reducing weight of inlet by 20-50% in compare with metal alloys [15]. This may lead to reduction in fuel consumption and, as a result, increased payload and range of the flight. Regarding the manufacturing it is suggested to manufacture inlet as combination of multiple large parts rather than a single part. The composite material could be manufactured as thick composite sheets and then assembled together using screw into the needed geometry. This would allow quicker and easier maintenance of the inlet. Table 2.5 shows the properties of CFRP. Figure 2.4 shows the CAD drawings of the inlet with design parameter dimensions.

Table 2.5: Carbon Fiber Reinforced Polymer Properties [6]

Parameter	Value
Maximum Service Temperature [K]	415
Density [kg/m^3]	1605.434
Tensile Strength [GPa]	1.1
Young Modulus [GPa]	131.96

3. COMPRESSOR

The compression system of the METU-PHOENIX engine relies on a two-spool design. The compressor consists of two stages of the fan and seven stages of the high-pressure compressor (HPC). METU-PHOENIX engine's compressors focus on providing the desired design pressure requirement in an efficient, light, and high-performance technique. Initial choices of material and manufacturing configurations of the compressor were considered to provide easier assembly and maintenance. AxSTREAM was used for the turbomachinery conceptual design.

3.1 Design Approach

The general approach for the compressor design is focused on achieving the requirements needed. Thus, a design guideline was created and followed. Table 3.1 shows the design guideline parameters and their typical range and limitations as stated in [5] and the RFP.

Table 3.1: Compressor Design Guideline

Parameter	Typical Range
Polytropic Efficiency	$0.85 \leq e_c \leq 0.92$
Flow Coefficient	$0.30 \leq \phi \leq 0.90$
Degree of Reaction	$0.10 \leq^\circ R \leq 0.90$
Working Coefficient	$0.20 \leq \psi \leq 0.50$
De Haller Criterion	$W2/W1 \geq 0.72$
Stage Average Solidity	$1.00 \leq \sigma \leq 2.00$
Stage Average Aspect Ratio	$1.00 \leq AR \leq 4.00$
Fan Aspect Ratio	$2.00 \leq AR \leq 5.00$
HPC Aspect Ratio	$1.00 \leq AR \leq 4.00$
HPC Max. Exit Temperature [K]	900

By using AxSTREAM, and after adding the boundary conditions obtained from GasTurb as the input, potential design points were found. Studying those design points, and by eliminating the ones that did not satisfy the design guideline, the ideal design point is chosen and used for the engine. The boundary parameters and their values obtained from GasTurb are shown in Table 3.2.

Table 3.2: Compressor Boundary Conditions From GasTurb

Parameter	Fan Inlet	Fan Outlet	HPC Inlet	HPC Outlet
Total Pressure [kPa]	75.07	127.62	126.35	1175.05
Static Pressure [kPa]	376.98	447.84	447.84	893.71
Total Temperature [K]	398.83	469.73	469.73	899.91
Mass Flow Rate [kg/s]	185.78		57.35	
Shaft Rotational Speed [RPM]	4882		8818	

It is good to mention that the process of turbomachinery was done by working alongside with GasTurb in an iterative process to ensure that the results obtained from both software are within a tolerance range of matching each other and to the design guideline created.

3.2 Fan

The fan is designed to provide a total pressure ratio of 1.69. As the compression ratio at outer and inner LPC are slightly different, in order to have single inlet and outlet boundary condition for the fan, total pressures at stations 13 and 25, see Figure 1.5, are mass flow averaged and was inserted into AxSTREAM. Using the inlet and outlet boundary conditions obtained from the GasTurb cycle analysis, the turbomachinery team decided to

design a two stage fan for the best fuel consumption conditions. It was decided also to dispense with the IGV (Inlet Guide Vane) to save on the engine weight as velocity triangles give satisfactory 1st stage rotor incidence without IGV for the given RPM.
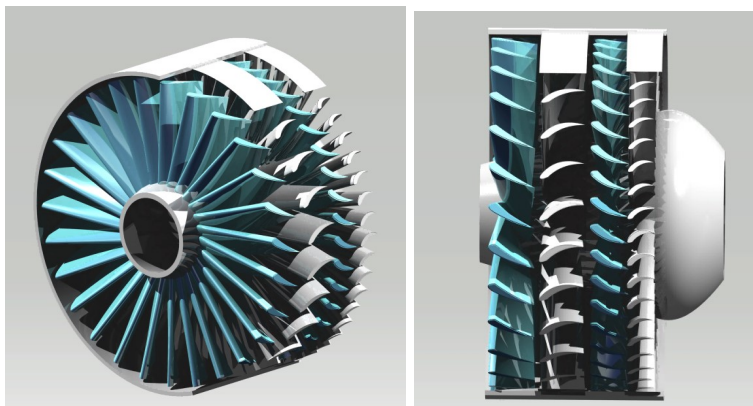
Figure 3.1: METU-PHOENIX Isometric and Side View of The Fan

3.2.1 Fan Results

Details of some important parameter values for each stage of the fan are provided in Table 3.3. Referring to Table 3.1, it can see that the values are within the ranges provided in the guideline.

Table 3.3: Important Design Parameters of The Fan

Parameter	Stage 1		Stage 2	
	Rotor	Stator	Rotor	Stator
Mass Flow Rate [kg/s]	185.78			
Axial Length [m]	0.83			
Flow Coefficient	0.69		0.64	
Work Coefficient	0.64		0.55	
Polytropic Efficiencey	0.88		0.94	
Isentropic Efficiencey	0.88		0.94	
Diffusion Factor by De Haller	0.72		0.72	
Equivalent Diffusion Factor	1.80		1.80	
Total-Total Pressure Ratio	1.32		1.28	
Flow Angle at Inlet [deg.]	0.4	-	-	-
Averaged Exit Mach Number	0.57	0.44	0.61	0.40
Solidity	1.29	0.59	1.24	1.40
Aspect Ratio	2.46	2.21	2.27	2.14
Degree of Reaction	0.66	0.33	0.46	0.53
Stagger Angle [deg.]	45.52	24.57	39.24	29.40
Inlet Metal Angle [deg.]	32.59	47.27	36.18	42.51
Outlet Metal Angle [deg.]	56.35	83.61	65.32	78.68
Tip Diameter [m]	1.60	1.56	1.54	1.51
Mean Diameter [m]	1.1	1.1	1.1	1.1
Hub Diameter [m]	0.59	0.64	0.65	0.68
Mean Diameter to Blade Height Ratio	2.40	2.47	2.65	2.77
Number of Blades	22	10	22	25

A close look at the fan sections, and their blades velocity triangles are shown in Figure 3.2.
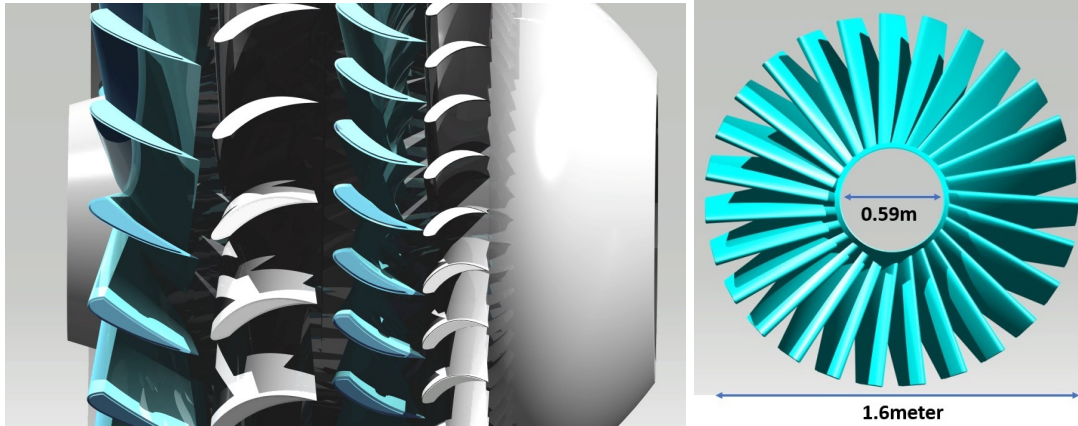
Figure 3.2: METU-PHOENIX Engine's Fan Close Look (Left) First Rotor Ring (Right)

3.3 High Pressure Compressor

Following the same procedure used in designing the fan, by importing the boundary conditions from GasTurb to AxSTEREAM, and by conducting comparisons between the different design points obtained from AxSTREAM and comparing them to the guideline given in Table 3.1, the HPC was decided to have 7 stages with a total-to-total pressure ratio of 9.30. For the similar reason with fan, IGV is not used in HPC.
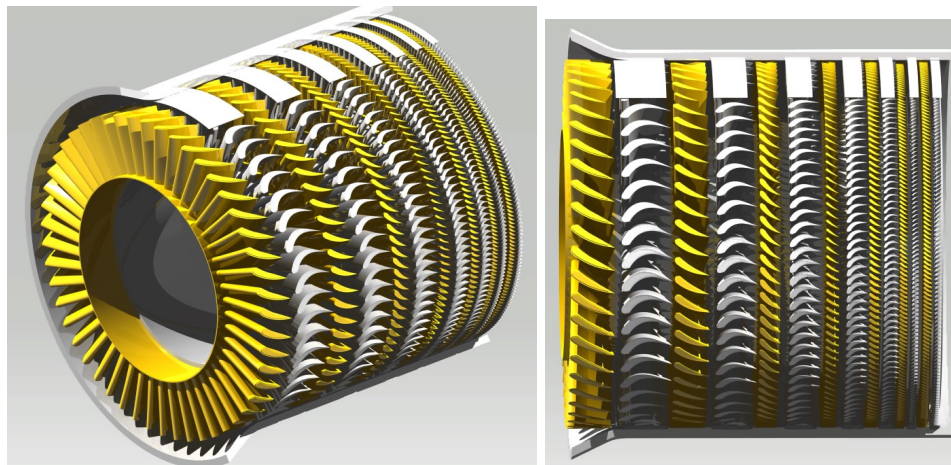
Figure 3.3: METU-PHOENIX Isometric and Side View of The HPC

3.3.1 HPC Results

The values of some important design parameters of the HPC are within the range defined in Table 3.1 for the selected design point. Those important parameters are listed in Table 3.4 along with the additional values obtained.

Table 3.4: Important Design Parameters of The First Four Stages of The HPC

Parameter	Stage 1		Stage 2		Stage 3		Stage 4	
	Rotor	Stator	Rotor	Stator	Rotor	Stator	Rotor	Stator
Mass Flow Rate [kg/s]	57.16							
Flow Coefficient	0.25		0.32		0.38		0.44	
Work Coefficient	0.34		0.37		0.40		0.43	
Polytropic Efficiencey	0.89		0.90		0.91		0.90	
Isentropic Efficiencey	0.88		0.89		0.90		0.90	
Diffusion Factor by De Haller	0.75		0.75		0.75		0.75	
Equivalent Diffusion Factor	1.86		1.86		1.86		1.86	
Total-Total Pressure Ratio	1.68		1.62		1.58		1.53	
Flow Angle at Inlet [deg]	2.8	-	-	-	-	-	-	-
Averaged Exit Mach Number	0.47	0.35	0.63	0.39	0.67	0.44	0.71	0.47
Solidity	1.99	1.73	1.99	1.99	1.99	1.99	1.99	1.99
Aspect Ratio	2.04	1.68	1.64	1.40	1.37	1.21	1.19	1.10
Degree of Reaction	0.85	0.14	0.67	0.32	0.65	0.37	0.57	0.42
Stagger Angle [deg]	69.13	37.49	58.90	38.99	51.88	38.28	44.88	37.74
Inlet Metal Angle [deg]	14.18	37.98	22.16	33.78	26.78	35.90	31.31	37.48
Outlet Metal Angle [deg]	27.53	67.02	40.03	68.21	49.43	67.52	58.91	67.03
Tip Diameter at Inlet [m]	0.86	0.81	0.79	0.76	0.75	0.74	0.73	0.72
Mean Diameter at Inlet [m]	0.69	0.69	0.69	0.69	0.69	0.69	0.69	0.69
Hub Diameter at Inlet [m]	0.53	0.57	0.59	0.62	0.63	0.65	0.65	0.66
Mean Diameter to Blade Height Ratio	5.79	7.16	9.64	11.94	15.61	19.01	24.03	28.95
Number of Blades	54	53	74	85	103	119	143	167

It is important to note that due to the EDU License of AxSTREAM provided, any design is limited to five stages, for that reason, the detailed values of the HPC are only provided for the first four stages however, the overall values for the full HPC, which consists of seven stages, are provided in the Table 3.5.

Table 3.5: Important Design Parameters of The HPC

Parameter	HPC Overall
Polytropic Efficiency	0.90
Isentropic Efficiency	0.85
Mass Flow Rate [kg/s]	57.16
Flow Angle at Inlet [deg.]	87.20
Averaged Flow Coefficient	0.62
Averaged Work Coefficient	0.31
Diffusion Factor by De Haller	0.75
Equivalent Diffusion Factor	1.86
Number of Stages	7
Max. Mach Number	1.44
Axial Length [m]	0.49
Min. Hub Diameter [m]	0.53
Max. Hub Diameter [m]	0.68
Min. Tip Diameter [m]	0.70
Max. Tip Diameter [m]	0.86
Exit Static Temperature T_3 [K]	900
Exit Total Pressure P_{03} [kPa]	1175.05

A close look at the HPC sections, and their blades velocity triangles are shown in Figure 3.4.
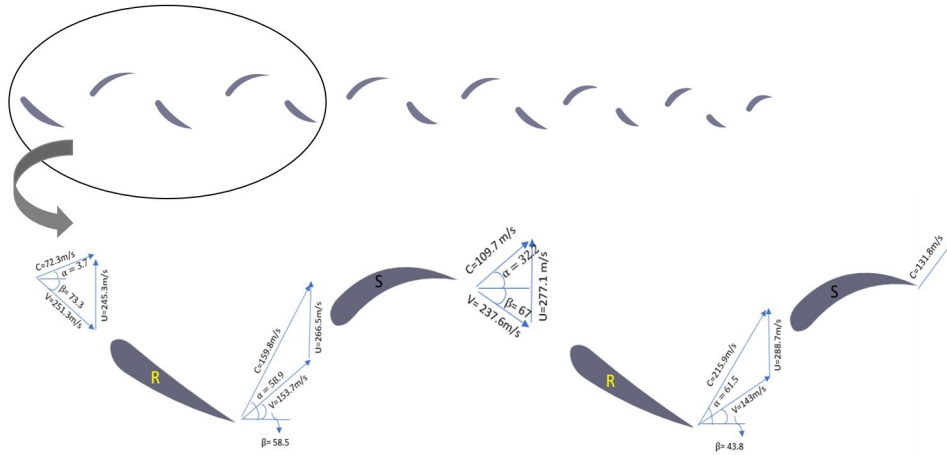
Figure 3.4: HPC Velocity Triangles
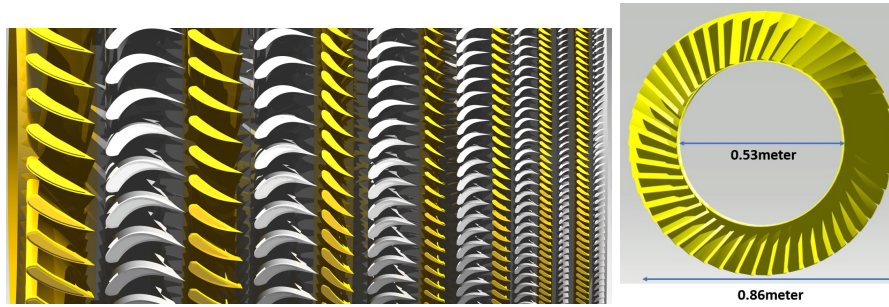
Figure 3.5: HPC Side View (Left) , HPC Ring (Right)

3.4 Off-Design Performance of Fan and HPC

Just as important as the design point of the compressor is, its off-design which is take-off condition at this report should be analyzed as well. Therefore, GasTurb software's Off-Design option is used to generate compressor maps. However, it was noticed that the LPC and HPC operating points beyond the scope of their maps, so the respective design point is moved to a more central point and both compressors maps re-scaled. Figure 3.6 show the compressor maps where circle point represents the design point and yellow rectangular stands for take-off condition.
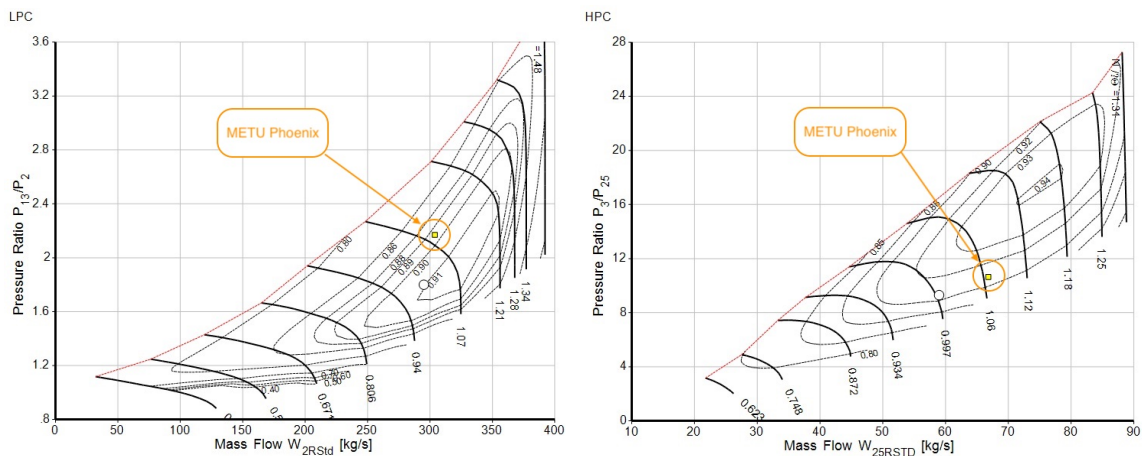
Figure 3.6: Off-Design Compressor Maps: Fan (Left) , HPC (Right)

It worth to mention that it was noticed that off-design point is hovering around 95%-110% of the corrected velocity but it is located at a point quite far from the stall margin. The team believe that this slight offset can be improved in the design processes to be conducted in the future by performing more detailed tests; however, for a preliminary design stage of the turbomachinery, the results obtained are acceptable. Future plans in turbomachinery optimizations will be discussed later.

3.5 Material and Manufacturing

The primary stresses that occur in the compressors are the centrifugal stresses in the rotors and their disks. Secondary stresses in the compressors include bending, vibration and thermal stresses. Therefore, using Equation 3.1, the stresses and required strength for each stage of fan and compressor is calculated using a simple MATLAB script.

$$\frac{\sigma_c}{\rho_{blade}} = \omega^2 \frac{A_z}{4\pi} \left[1 + \frac{A_t}{A_h}\right] \tag{3.1}$$

Additionally, the maximum temperature that each stage will resist is also found from turbomachinery analysis and its results are shown in Table 3.6.

Table 3.6: Compressor Stress Analysis

Variables	Fan		HPC						
	Stage 1	Stage 2	Stage 1	Stage 2	Stage 3	Stage 4	Stage 5	Stage 6	Stage 7
Req. Material Strength to Density Ratio $(/10^4)$ $[Pa/(kg/m^3)]$	30.324	21.152	8.821	5.252	3.534	2.545	1.928	1.516	1.233
AN2 Rule $(/10^7)$ $[(m*rpm)^2]$	4.159	3.665	2.544	1.969	1.523	1.191	0.948	0.771	0.642
Maximum Temperature [K]	250	389	395	453	521	596	684	784	900

3.5.1 Fan's Material and Manufacturing

METU-PHOENIX engine's fan will be made of AVIMID® N as it has the service temperature of roughly 643 K and sufficient mechanical properties for the design purposes. It is common that fan is consisting a large portion of overall engine weight and since AVIMID® N has a quite low density in compare with other competitive materials, it seems as an appropriate option for fan's material which can help METU-PHOENIX engine to have low weight in the market in compare with similar competitors.

Table 3.7: AVIMID® N, Material Properties [7]

Parameter	Value
Maximum Service Temperature [K]	643
Density [kg/m^3]	1450
Tensile Strength [MPa]	110
Young Modulus [GPa]	4.1

3.5.2 Compressor's Material and Manufacturing

State-of-the-art HPC's commonly have a design with the first five stages made out of titanium blisks which being machined using CNC, and the following stages are utilizing a design with nickel blades insert. Since Concorde is a supersonic aircraft that is capable of flying at high Mach numbers, because of high temperatures, only the first three stages would be made of Ti-834. The latter four stages feature compressor blisks made of Ti48A12Cr2Nb, a highly durable titanium-aluminum alloy against extremely high temperatures.

It is necessary to mention that utilizing blisks for HPC rotors can reduce the weight of compressors by approximately 20-30%. Additionally, it can enhance the number of parts in the HPC system, which can lead to easy assembly and maintenance. The turbomachinery team considered using blade fir-tree design since they provide easier assembly, especially when a specific rotor is damaged, it can be replaced easily without changing the whole disk, providing less maintenance time and cost; however, due to the extreme loading caused by the centrifugal loading on the blades, especially in the turbine, it was decided that blisks design is more suitable to ensure better performance and provide better security of rotor failure [16].
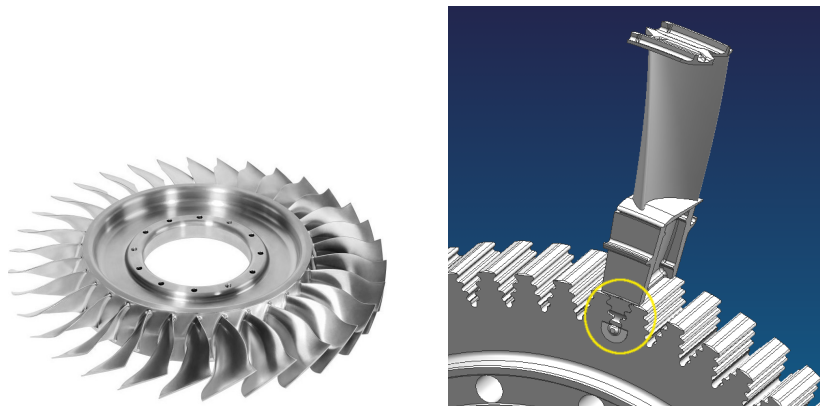
Figure 3.7: Blisk vs. Fir-Tree Designs

Since the latter 4 stages blade height are very small, it is quite hard to manufacture them using traditional CNC methods. Therefore, it is suggested that to use 3-D printing methods post-processing with electron beam welding (EBW) [8].

Table 3.8: Fan & Compressors Material Properties [8]

Parameter	Ti-834	Ti48A12Cr2Nb
Maximum Service Temperature [K]	872	1110
Density [kg/m^3]	4550	3900
Tensile Strength [MPa]	110	296
Young Modulus [GPa]	120	170

4. COMBUSTION CHAMBER

Combustion chamber is the component where the temperature of pressurized air coming from compressor is increased further and diverted to nozzle guide vanes. Air coming from station 3 , see Figure 1.1, is diffused first before going in to the chamber, it, then, splits into three parts. Some amount enter directly to flame tube via dome and swirler where it is mixed with fuel to burn in primary zone. Other part travels through outer and inner annuli to mix with flame tube flow and cool its walls. Main jet streams at outer and inner wall penetrate into the combustion products to further enhance mixing process and circulation zones are created. This process continues until secondary zone. Finally, temperature of the flow is decreased to desired levels at the end of dilution zone.

There are certain constraints that must be satisfied for a safe and efficient combustion. In an aero-engine the speeds inside the engine compared to other applications of turbo machines is relatively higher. That is why the air passing through the combustion chamber is needed to be burnt in a short period of time and the stability of the flame should be conserved while doing so. Volume and length of the flame tube is considered as a determinant factor in this aspect.

4.1   Combustion System Design

This section presents the METU-PHOENIX engine's combustion chamber, which is where the air and fuel mixture is burned. The role of good mixing in achieving a high combustion efficiency cannot be overstated. It should be remembered that a highly efficient combustion chamber can be achieved by rapidly atomizing liquid fuel into very small droplets [1]. The required form of swirler should be chosen based on the specifications in order to achieve sufficient droplets.
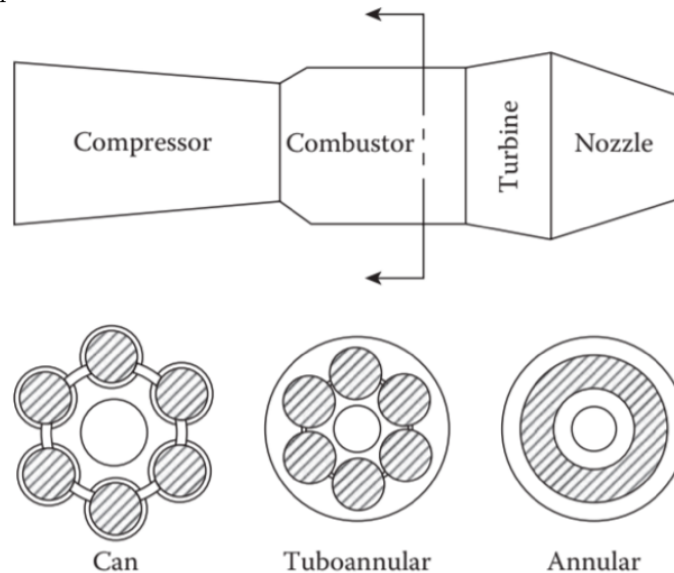
Figure 4.1: Types of Combustion Chambers [1]

Can, Tuboannular, and Annular Combustors are the three different types of combustion chambers shown in Figure 4.1. The METU-PHOENIX engine uses an annular premixed Hybrid Diffuser combustion chamber to fit the aerodynamic configuration with the compressor outlet flow and minimize pressure loss [1], which is similar to what current commercial aircraft engines like the GE90, CFM-56, and GEnx use. Furthermore, compared to other types, the annular combustion chamber produces more uniform combustion, has a smaller surface area, and is smaller in size. For the METU-PHOENIX engine, an annular type combustion chamber was chosen based on the advantages mentioned above.

4.1.1 Design Point Selection

The cycle analysis design and off design points are selected as the combustor design point. The combustor inlet conditions for the design point are taken from the cycle and compressor designs and specified in the Table 4.1.

Table 4.1: Combustor Inlet Conditions

Parameter	Symbol	Value	Reference
Air Mass Flow at Inlet [kg/s]	m_3	55.3925	Compressor Design
Total Temperature at Inlet [K]	T_3	900	Cycle design
Static Temperature at Inlet [K]	$T_{(s,3)}$	893	Compressor Design
Total Pressure at Inlet [kPa]	$P_{(t,3)}$	1175.05	Cycle Design
Static Pressure at Inlet [kPa]	P_3	1143.96	Compressor Design
Air Density at Inlet [kg/m^3]	ρ_3	4.45921	Compressor Design
Area at Inlet [m^2]	A_3	0.105745	Compressor Design
Ratio of specific heats	γ	1.4	Compressor Design
Universal Gas Constant [J/(kg K)]	R	287.05	Cycle Design
Mach Number at Inlet	M	0.41	Compressor Design
Specific Heat [J/(kg K)]	C_p	1120.88	Compressor Design
Velocity at Inlet [m/s]	V	247.79	Compressor Design
Pressure Ratio of Burner	π_b	0.96	Cycle Design

4.1.2 Diffuser Design

Because the axial flow velocity of a compressor is high as 247.79 m/s ($M = 0.41$), this velocity must ideally be lowered over a short distance until combustion takes place. A diffuser is placed between the compressor exit and the burner inlet to achieve this flow reduction.

The design objective of the diffuser is to reduce $M = 0.2$ the air velocity that exits the compressor as much as possible , to ensure optimum combustion efficiency for the lowest loss of overall air pressure [5]. Unfortunately, the number of design and performance parameters for annular flat-wall diffusers is very limited. The various forms of diffusers are shown in the Table 4.2.

It is determined to pick a hybrid configuration for the METU-PHOENIX engine after analyzing Table 4.2. The hybrid diffuser can achieve a static pressure recovery of at least 25% as opposed to traditional diffusers of the same length because it combines a vortex-controlled diffuser with a conventional wide-angled post-diffuser located at the exit.

Table 4.2: Types of Diffusers [1]

Diffuser Type	Advantages	Disadvantages
Aerodynamic or faired	-Low pressure loss	-Relatively long -Performance susceptible to thermal distortion and manufacturing tolerances -Performance and stabilitysensitive to variations in inlet velocity profile
Dump	-Relatively short -Insensitive to variations in inlet flow conditions	-Pressure loss about 50% higher than for faired type
Vortex-controlled	-High performance -Short length -Low pressure loss	-Requires minimum of 4% air bleed -Design procedures not fully established
Hybrid	-High performance -Short length -Low pressure loss -Low bleed air requirement	-Design procedures not fully established -Bleed air pressure too low for turbine cooling

According to [2] , the best possible flat-wall diffuser has a $2\theta = 9$ degree included angle. Also, When the Diffuser area ratio is less than 4, the excess length of the diffuser can be decreased by splitting the flow into adjacent streams, each with an included angle $2\theta = 9$, as seen in Figure 4.2. The needed length for any AR< 4 is decreased by a division factor equal to the number of parallel streams, in this case three in the case of two splitter plates as seen in Figure 4.2. The number of splitter plates could theoretically be expanded to three, four, five, or six, resulting in a shorter diffuser. However, due to the geometric sophistication and manufacturing difficulties of this solution, two splitter vanes seem to be the best option [2].
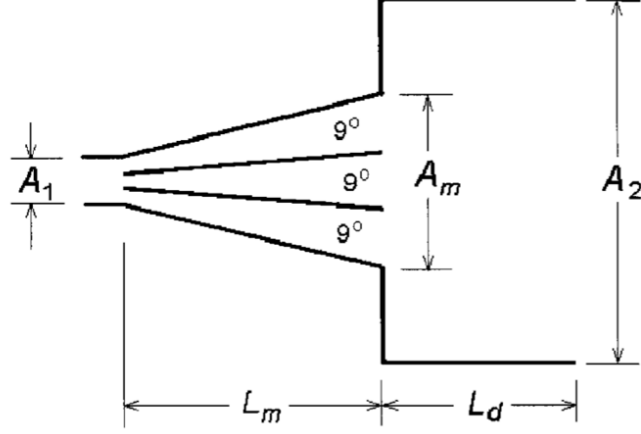
Figure 4.2: Combined Diffuser [2]

According to Mattingly's method, the total pressure loss coefficient is calculated as in Equation 4.1.

$$(\Delta P_t/q_1)_D = (1 - 1/AR^2)(1 - \eta_D) \tag{4.1}$$

Under the assumption of a uniform, stable, incompressible flow of zero friction, Equation 4.2 calculates the total pressure loss of the annular flat-wall diffuser with two splitters plates.

$$\Delta P_t = q_1(1 - 1/AR^2)(1 - \eta_D) \tag{4.2}$$

Where q_1 is the inlet dynamic pressure of combustor, η_D is the best efficiency of the whole diffuser combined by the flat wall diffuser and dump diffuser and AR is the area ratio. η_D can be calculated as in Equation 4.3.

$$\eta_D = (\eta_{D9°}AR^2(1 - [A_1/A_m]^2) + 2(AR[A_1/A_m] - 1))/(AR^2 - 1) \tag{4.3}$$

Where $\eta_{D9°}$ is the best efficiency of the flat wall diffuser with expansion angle $2\theta = 9°$ According to [2], it is chosen as $\eta_{D9°} = 0.9378$, from Equation 4.4.

$$\eta_{D9°} = 0.965 - 2.72B_t \tag{4.4}$$

Where B_t is the thickness of the turbulent boundary layer at diffuser entry.

According to Mattingly, total pressure ratio is calcualted as in Equation 4.5.

$$\pi_D = 1 - (1 - 1/AR^2)(1 - \eta_D)/(1 + 2/(\gamma M_1^2)) = 0.99 \tag{4.5}$$

1% loss is calculated after measuring pressure drop across the diffuser. As a result, according to [2] this is valid.

Table 4.3 is a list of the geometry parameters and the calculated results.

Table 4.3: Pre-Diffuser Calculated Parameters

Parameter	Symbol	Value	Reference
Diffuser Inlet Area [m^2]	A$_1$	0.106	Compressor Design
Diffuser Flat Wall Area [m^2]	A$_m$	0.314	Calculated
Diffuser Exit Area [m^2]	A$_2$	0.335	Calculated
Total Pressure at Diffuser Inlet [kPa]	P$_{t,31}$	1175.05	Compressor Design
Pressure Loss in the Diffuser [kPa]	ΔP	6.874	Calculated
Total Pressure at Diffuser Exit [kPa]	P$_{t,32}$	1168.18	Calculated
Length of the Diffuser [m]	L	0.309	Calculated
Mach Number at Diffuser Exit	M$_{3,2}$	0.2	Calculated
Efficiency of flat Wall diffuser	η_{D9°	0.938	Calculated
Efficiency of the diffuser	η_D	0.94	Calculated
Area Ratio	AR	3.16	Calculated

4.2 NOx Emissions

Another important consideration in the combustion chamber's configuration is NOx emissions. It is important to have enough time and temperatures while reactions occur in order to design a low-emission combustion chamber. Reducing the equivalence ratio of the primary zone to achieve lean-burn combustion, improving injector performance by better atomization, reducing the residence time of high temperature combustion chamber gas, and improving the uniformity of the fuel-air mixture are the four main considerations to to take into account when designing a combustion chamber [17] [18].

Three types of the currently used major low-emission combustion chambers in aeroengines which are LDI(Lean Direct Injection),LPP (Lean Premixed Prevaporized Combustion) and RQL(Rich burn - quench - lean burn) and are given in Table 4.4.

Table 4.4: Comparing between different low emission methods[9]

Low emision method	LPP	RQL	LDI
NOX emission	Extremely low	Very low	Very low
Combustion efficiency	Extremely high	High	High
Combustion stability	Flash back Combustion unstable Spontaneous combustion	No flash back	Combustion unstable
Smoke	Extremely low	High	Low
Configuration	Short length	Long length	Short length Complex dome
Development prospect	Common	Good	Best

Based on Table 4.4 and the RFP specifications, it was chosen to go with the LDI configuration because of its low NOx emission and little smoke formation, as well as its high combustion efficiency and short length. Furthermore, LDI configuration is compact and lightweight.

4.3 Volume and Efficiency

For certain operations of the engine, maximum take-off rating as being one of the critical ones, there is a minimum value of combustion chamber volume to sustain efficient burning. Knowing the compressor exit flow properties, combustion loading and intensity values can be found for a given volume. Equations 4.6, 4.7 represent combustion loading and intensity respectively. Efficiency can be approximated as a function of combustion loading [4].

$$CL = \frac{W_3}{VP_3^{1.8}10^{0.00145(T_3-400)}} \tag{4.6}$$

$$CI = \frac{W_f\eta_bQ_R}{P_3V} \tag{4.7}$$

Loading and intensity values have maximum limits for safe operation which sets a minimum required flame tube volume. Using the station 3 flow properties and solving Equations 4.6 and 4.7 for V, volume can be initialized with assigned loading and intensity.

At maximum altitude and minimum Mach number operation within the flight envelope, loading should be less that 50 $kg/(s.atm^{1.8}.m^3)$ for weak extinction margin with acceptable efficiency. At sea level static maximum rating intensity should be less than 60 $MW/(atm.m^3)$ [4]. Both the operating point data are taken from performance calculations. For the maximum altitude minimum Mach number flight, input to performance calculation is given with respect to Figure 4.3. It corresponds approximately to 60 thousand feet with Mach 1.4 [19]. The output from performance can be seen in Table 4.5. Cruise values of station 3 is tabulated as well to refer later for design point.
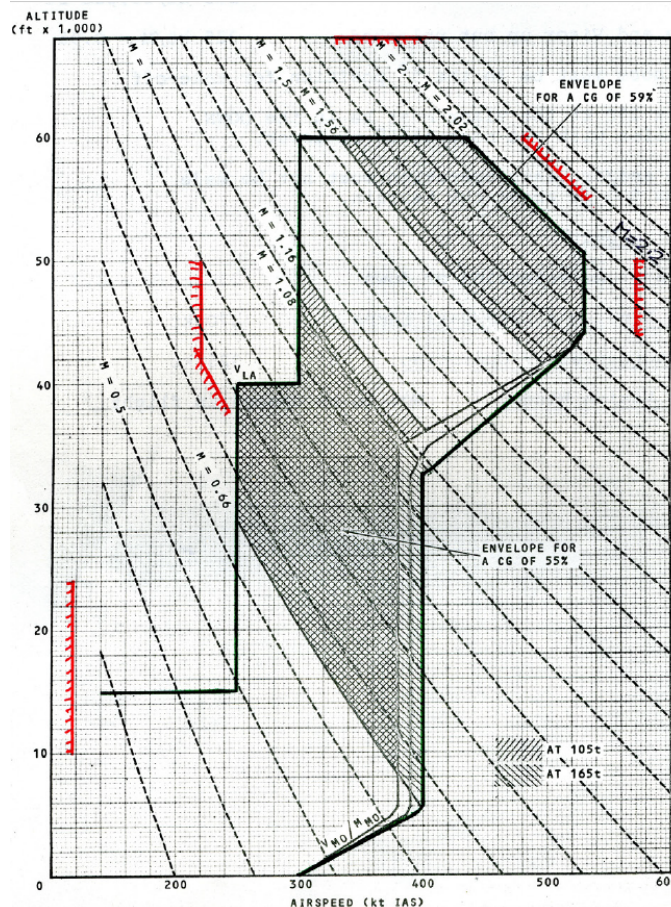
Figure 4.3: Concorde flight envelope [3]

Table 4.5: Station 3 properties

(a) Maximum altitude, minimum Mach

Property	Value
T_3 [K]	791
P_3 [kPa]	496.55
W_3 [kg/s]	24.28
W_f [kg/s]	0.57

(b) Sea level static MTO

Property	Value
T_3 [K]	806
P_3 [kPa]	2417.15
W_3 [kg/s]	118.5
W_f [kg/s]	2.73

(c) Cruise

Property	Value
T_3 [K]	900
P_3 [kPa]	1175.06
W_3 [kg/s]	55.4
W_f [kg/s]	1.24

Efficiency is obtained from Figure 4.4. Unconstrained design curve is curve-fitted and 6th order polynomial is created so that η_b is kept up to date for any value of loading. First the volume is calculated according to allowed maximum loading and intensity values with respect to the mentioned operating points. The minimum volume obtained among them is picked and substituted to the other one to check if the volume satisfies both of them. If not, volume is iterated and η_b is updated.
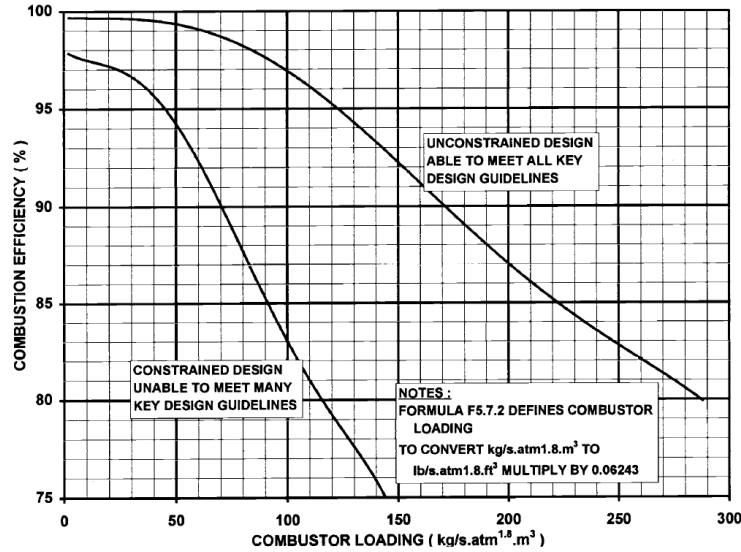
Figure 4.4: Concorde flight envelope [4]

It is observed that the iteration for increasing the volume kept on just to satisfy the limit for combustion intensity at MTO. From the obtained volume, variables are calculated in MATLAB again for cruise conditions and shown in Table 4.6.

Table 4.6: Cruise conditions

Volume [lt]	CL cruise [kg/(s atm$^{1.8}$ m^3)]	CI cruise [MW/(atmm^3)]	η_b
87.2 liters	4.85	52.46	99.5

4.4 Fuel Atomizing Flow

Usually, an air-blast atomizer needs 3 lbm of primary air for per lbm of fuel [2]. Table 4.7 lists the fuel atomizing flow and other associated parameters.

Table 4.7: Fuel Atomizing Flow Calculation

Parameter	Symbol	Value	Reference
Mass flow rate at burner inlet [kg/s]	W_3	55,4	Cycle design
Fuel flow rate [kg/s]	W_f	1.24	Cycle design
Atomize Air to Fuel ratio	AFR	3	Mattingly
Fuel Atomizing airflow calculation [kg/s]	W_{af}	3.73	Combustor design

4.5 Sub-components Design Approach

For the sub-components of the combustion chamber preliminary design, following references are used as the road map, [20] [4] [21]. First a flow split analysis is made, from the equal amount of mass flow going through the outer and inner annulus, outer and inner radii of the flame tube is determined. Outer casing radius is determined from turbine AxStream data. A constraint to ratio of flame tube height to length is given as an input to combustion chamber design from performance data as 0.4 and let varied ±0.001. This sets the length of the tube for a given height.

For a given Mach number and flow properties, area can be calculated using mass flow parameter formula, in Equation 4.8. Hot flow γ and c_p are taken as 1.33 and 1157 J/kg/K respectively and cold flow values are 1.4 and 1005 J/kg/K. Gas constant for air is taken as 287 J/kg/K throughout the calculations.

$$Q = \frac{W_3\sqrt{T_3}}{P_3 A_3} = \frac{\gamma}{R} M \left(1 + \frac{\gamma - 1}{2} M^2 \right)^{\frac{-\gamma - 1}{2(\gamma - 1)}} \tag{4.8}$$

Jet stream calculations are tried to be done with least amount of input. In that manner the designer team came up with an idea and the simplest way to describe it is, with an example. Let us say, number of injectors is 15, so for an annular combustion chamber 360° is divided into 15° for the hole calculations. With the known outer and inner flame tube radii, the arc length these surfaces cover can be calculated. Number of hole diameters these lengths comprise is given as an input. Second input is how many holes at that surface are going to be.

With the help of that procedure, number of hole sizing input for both primary and secondary zone is five, being N_{injector}, PZN_{hole}, PZH_{diameter}, SZN_{hole} and SZH_{diameter}. This procedure results in smaller holes at inner wall of flame tube and lets more lower annulus mass flow to the dilution zone which could reduce the flow temperature at the hub. Since the turbine hub is subjected to high mechanical stress due to high RPM, reducing the thermal stress is beneficial for its operation.

Holes are designed to be plain for simplicity. Flow coming from annulus is parallel to the plain of holes and pressure differential between the volumes create the jet stream. Due to the viscous effects and different flow directions, W_j is calculated with the addition of discharge coefficient, C_D. An analytical relation for the approximation of behaviour of jet stream is used for the preliminary analysis [21].

$$V_{jet} = \sqrt{\frac{2\gamma}{\gamma - 1} RT \left[1 - \left(\frac{P}{P_0} \right)^{\frac{\gamma - 1}{\gamma}} \right]} \tag{4.9}$$

Pressure ratio at the right hand side of Equation 4.9 is obtained from performance calculations as an input.

In order to determine the C_D, Equations from 4.10 to 4.13 are used.

$$\alpha = \frac{W_j}{W_{annulus}} \tag{4.10}$$

$$K = 1 + \frac{\Delta P}{q_{annulus}} \tag{4.11}$$

$$C_D = \frac{1.25(K - 1)}{[4K^2 - K(2 - \alpha)^2]^{0.5}} \tag{4.12}$$

Where $q_{annulus}$ is the dynamic pressure of the annulus flow. Finally, W_j can be calculated as in Equation 4.13.

$$W_j = C_D A_j \rho_j V_j \tag{4.13}$$

Where A_j is calculated from number of holes and their diameters, ρ_j from annulus flow properties. This is an iterative process as W_j is not known at the first place at Equation 4.10. Taking C_D as one for the first iteration, it converges to a final value. It was observed that the three iterations are enough to converge to a relative percentage error of $2.5 \times 10^{-5}\%$ which is the largest among four hole calculations.

Once the mass flow through the jet holes is known, the length of the penetration can be calculated. Since the mass flow through the outer and inner annulus are the same and the hole diameters are different, holes at different radii do not result in the same penetration. Lower and outer jet penetrations are averaged and this value is tried to be equated to the mid section of the flame tube. Equation 4.14 shows the penetration of multiple jets [21].

$$Y_{max} = 1.25 d_j \sqrt{J} \frac{W_g}{W_g + W_j} \tag{4.14}$$

$$J = \frac{\rho_j V_j}{\rho_g V_g} \tag{4.15}$$

Subscript g, corresponds to gas, flow in the flame tube. It is found with the properties after combustion process in the relevant zone.

As part of flow split analysis, 15% of W_3 passes through swirler, 50% of jet stream participates in combustion, the other half mix with flame tube flow. 80% of fuel burns in primary zone, rest in the second. For the temperature calculations, energy balance equation is used. After the final flame temperature is obtained, it is mass flow averaged using other half of W_j. This procedure is formulated in Equations 4.16 and 4.17 for primary zone.

$$(W_{swirler} + \frac{1}{2}W_j + 0.8W_f)c_{p,hot}T_{final} = W_{swirler}c_{p,cold}T_3 + \frac{1}{2}W_jc_{p,cold}T_3 + W_fQ_R0.8 \qquad (4.16)$$

$$T = \frac{T_{final}(W_{swirler} + \frac{1}{2}W_j + 0.8W_f) + T_3\frac{1}{2}W_j}{W_{swirler} + W_j + 0.8W_f} \qquad (4.17)$$

T in Equation 4.17 is taken as the inlet flow temperature of secondary zone. Burner efficiency represents the percentage of fuel that is successfully used in combustion process. Since 80% of fuel was already consumed in PZ, leftover fuel, which is $(\eta_b - 80) = 19.5\%$, burns with the same procedure as in primary zone and flow is mixed further with the SZ jets. According to these calculations, some amount of W_3 is mixed theoretically with final combustion products as dilution air to give the station 4 temperature given as 1721 K from performance calculations.

Heat transfer analysis between flow and liner wall is out of the scope of this report. Some amount, percentage, of W_3 is allocated for cooling purposes. A percentage value is taken from literature [22] as goal and design is targeted such that the after dilution air is used to achieve desired T_4, leftover air is going to be used as coolant.

Residence time is calculated from secondary zone exit flow properties. Left hand side of Equation 4.8 is known after following the described procedure. Right hand side of the equation is plotted and a 6th order polynomial is fitted for a fast approximation of Mach number when the flow properties are known. From Mach number and temperature, velocity at the station is obtained. Since the overall length can be derived from the known volume and height of the flame tube, residence time is calculated by dividing length into velocity.

4.6 Sub-components Design Results

Formulas and the relations are integrated into Excel Work Sheet and Solver option is used with defined constraints and inputs with the goal of achieving T_4, they are shown in Table 4.8.

Table 4.8: Solver inputs and constraints

(a) Inputs

Inputs	
Outer casing R [mm]	480
Inner casing R [mm]	≤ 350
Annulus Mach	0.1 - 0.15
$N_{injector}$	15 - 30, integer
PZN_{hole}	2 - 5, integer
$PZH_{diameter}$ [mm]	≥ $PZN_{hole} + 1$
SZN_{hole}	2 - 7, integer
$SZH_{diameter}$ [mm]	≥ $SZN_{hole} + 1$

(b) Constraints

Constraints	
PZ Mach	≥ 0.01
PZ temperature [K]	≤ 2800
Residence time [ms]	3 - 8
$\left\| \frac{(PZY_{max}avg.) - R_{mid}}{R_{mid}} \right\| \%$	≤ 10
$\left\| \frac{(SZY_{max}avg.) - R_{mid}}{R_{mid}} \right\| \%$	≤ 10
Can H/L	0.4 ± 0.01
%W_3 for cooling	≥ 40

In Table 4.8(b) two mathematical formulas can be seen. They represent the averaged penetration of different zones, PZY_{max} for primary and SZY_{max} for secondary zone jets. The cells in the table is the percent distance of penetration relative to the mid plane of flame tube.

Table 4.9: Design combustion chamber parameters

Design Parameters			
T4 [K]	1721	PZ exit T [K]	2532
Volume [lt]	87.2	SZ exit T [K]	1973
Outer Casing R [mm]	480	PZ Mach	0.035
Inner Casing R [mm]	291	SZ Mach	0.037
Outer Flame Tube R [mm]	452	PZ Annuli Mach	0.104
Inner Flame Tube R [mm]	325	SZ Annuli Mach	0.079
Flame Tube Length [mm]	300	DZ Annuli Mach	0.066
Flame Tube Height [mm]	118	Residence time [ms]	7.6
Can H/L	0.393	CL_{cruise} [kg/s/atm$^{1.8}$/m^3]	4.85
$N_{injector}$	27	CI_{cruise} [kW/atm/m^3]	52.46
PZN_{hole}	5 outer, 5 inner	Flame tube mid plane [mm]	63.395
$PZH_{diameter}$ [mm]	13.131 outer, 9.447 inner	PZY_{max} avg. [mm]	63.025
SZN_{hole}	2 outer, 2 inner	SZYmaxavg. [mm]	62.890
$SZH_{diameter}$ [mm]	8.257 outer, 5.940 inner	%W_3 for cooling	40

Table 4.9 shows the design parameters obtained with explained procedures and constraints. There has been many simplifying assumptions and relations throughout the design steps. It is important to preliminary size the major dimensions in order to move on with 3D models, that are going to be simulated in computational fluid dynamics (CFD) programs, to both have a starting point and to converge to an optimum combination of parameters faster. Combustion simulations require considerable amount of computational power to predict the behaviour of the flow accurately which unfortunately something the designer team is lack of. Dimensions from Table 4.9 are used to draw the combustion chamber components in CAD environment and some isometric views are shown in Figure 4.5.

(a) Flame tube and casing

(b) Flame tube inner (down) and outer (up) walls

(c) Combustion chamber cross-section

(d) Flame tube
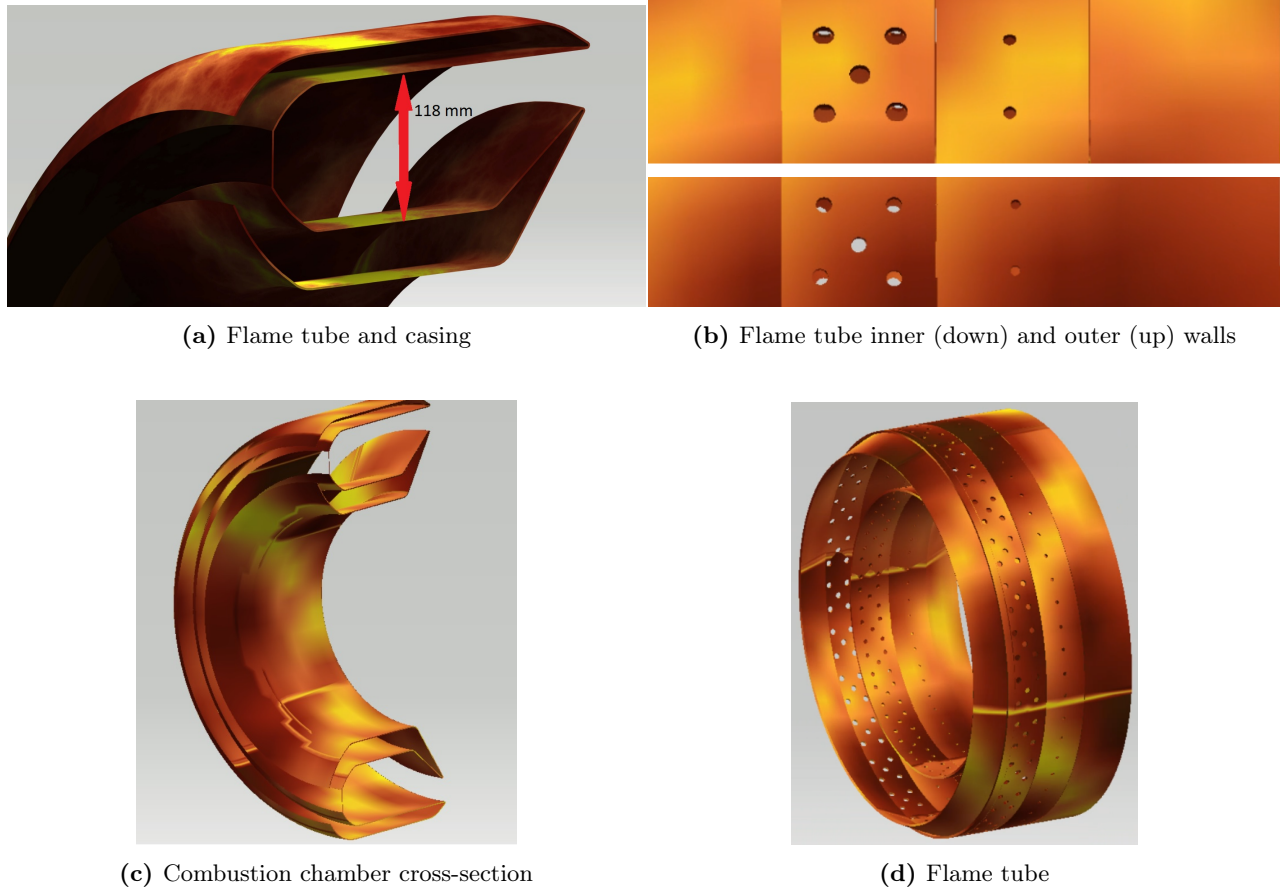
Figure 4.5: Isometric CAD drawings of the combustion chamber

4.7 Material and Manufacturing

Combustor is one of the major structural component of the engine that undergoes a lot of stress. It is in fact a pressure vessel and experiences the largest gauge pressure in the engine. The combustor casing will undergo the temperatures that similar to exit compressor discharge temperature. Thus, the combustor casing for the METU-PHOENIX shall be manufactured out of the same Ti-Al alloy used in the last 3 stages of the compressor. It will also be manufactured with a thermal coating barrier (TBC) such as yttria-stabilized zirconia (YSZ). Ceramic TBCs have a thermal conductivity almost 20 times lower than that of nickel alloys [23]. This allows a TBC part to experience a lower metal temperature compared to one with no coating. The combustor liner is decided to be made out of Ceramic Matrix Composites (CMC). The CMC components may be manufactured using a process called Polymer infiltration and pyrolysis (PIP). This method infuses a liquid preceramic polymer into the fiber preform. This process is simpler and relatively low cost compared to other CMC manufacturing methods such as CVD or melt infiltration [24]. Table 4.10 shows the CMC properties.

Table 4.10: CMC Properties

Parameter	Value
Maximum Service Temperature [K]	1670
Density [kg/m^3]	2100.90
Tensile Strength [MPa]	310
Young Modulus [GPa]	95

Maximum service temperature is in fact lower that the mentioned one in Table 4.9. However, cooling air prevents the liner walls from reaching those temperatures.

5. TURBINE

The METU-PHOENIX engine features two stages of HPT and a two stages LPT. In a 2-spool design, work is being extracted from hot air flow using HPT and high pressure compressors (HPC) are utilizing this power; on the other hand, the LPT is supplying the required power to the fan. Turbines, especially the nozzle guide vanes, are experiencing the highest temperature in the engine; therefore, turbines are considered as one of the most stressed components in any aero-engines. During turbine design major parameters that were taken into account such as efficiency, transmitted power, lifetime and weight.
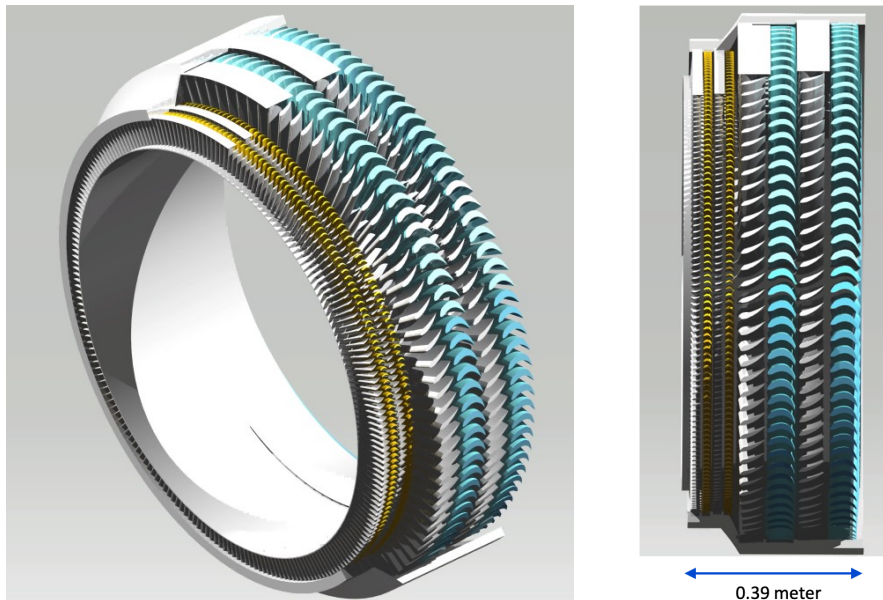
Figure 5.1: METU-PHOENIX Isometric and Side View of Turbine
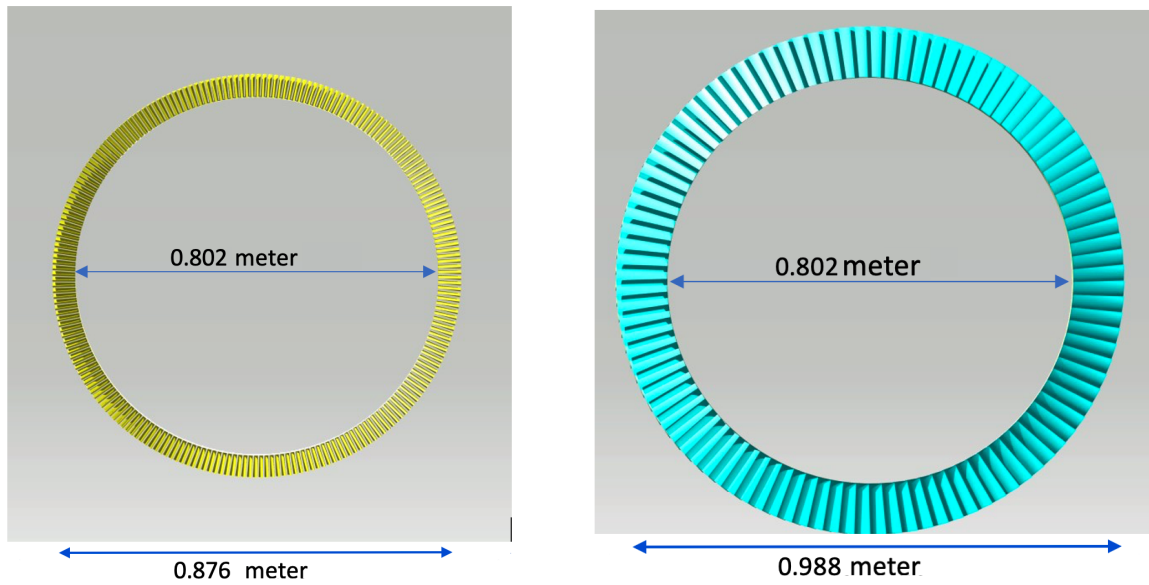
Figure 5.2: METU-PHOENIX HPT and LPT Ring Rotor

5.1 Design Approach

The general design approach started by defining the turbine design requirements and generating a design guideline. Table 5.1 shows general turbine design guideline that has been extracted from Mattingly, Farokhi, Sagerser and Denney [20][5][25][26].

Table 5.1: Turbine Design Guideline

Parameter	Typical Range
Zweifel Loading Coefficient	$0.80 < \xi < 1.00$
Flow Coefficient	$0.50 < \phi < 1.10$
Degree of Reaction	$0.20 <^\circ R < 0.70$
Loading Coefficient	$0.80 < \psi < 2.30$
AN^2 [(RPM $\times$ m)^2]	HPT: $AN2 < 5.5 * 10^7$ LPT: $AN2 < 6 * 10^7$
Exit Rotor Mach Number	$M_{r3} \approx 0.90$
Exit Nozzle Flow angle [deg]	$\alpha_2 < 70$
Exit Nozzle Mach Number	M_2 1.10

In the METU-PHOENIX engine, similar to compressor design approach, boundary conditions of turbines were retrieved from GasTurb and these values and ranges were imported into AxSTREAM and number of iterations were performed and wide range of potential design points were created. After indicating desired range for each parameter, potential design points were narrowed down and the point which satisfies the design criteria and has maximum efficiency for the turbine is chosen.

Table 5.2: Turbine Boundary Conditions From GasTurb

Parameter	HPT Inlet	HPT Outlet	LPT Inlet	LPT Outlet
Total Pressure [kPa]	1128.05	324.36	317.88	136.448
Static Pressure [kPa]	1064.96	1064.96	286.69	136.43
Total Temperature [K]	1721	1280	1268	1053
Mass Flow Rate [kg/s]	50.75		57.35	
Shaft Rotational Speed [RPM]	8813		4882	

5.2 High-Pressure Turbine

In the Table 5.2, thermodynamic properties that are obtained from GasTurb and the results that has been obtained by the AxSTREAM Turbomachinery calculations are shown and compared. Flow coefficient, Work coefficient, efficiencies and number of stages (weight) were major parameters that are considered during turbine design. It worth to mention that at the beginning, it was aimed to design a HPT with only one stage to reduce the weight of engine; It was observed that the loading coefficient must be approximately 2.1 when one stage is used which is a reasonable value as turbine blades accept much more loading without danger of boundary layer separation. However, it was noticed that engine has to work harder than it needed to. This lead to utilizing two stages and distribution the work load between stages.

5.2.1 HPT Design Results

Details of design parameters which has been obtained from AxSTREAM are given in Table 5.3. When each parameter is compared with its typical values, it is seen that the results are consistent with the values stated previously in the turbine design guideline, Table 5.1.

Table 5.3: Detailed Design Parameters of High Pressure Turbine

Variables	Stage 1		Stage 2	
	Stator	Rotor	Stator	Rotor
Flow Coefficient	0.50		0.96	
Stage Loading	1.81		1.39	
Degree of Reaction	0.29		0.34	
Power Extracted [MW]	13.43		9.77	
Isentropic Efficiency	0.91		0.90	
Zweifel Coefficient	0.67	0.77	1.09	0.98
Aspect Ratio	1.39	1.85	1.51	2.12
Solidity	1.36	1.47	1.34	1.45
Number of Blades	98	82	113	94
Stagger Angle [deg]	48.67	18.48	27.83	32.18
Inlet Metal Angle [deg]	79.58	39.15	65.68	75.46
Outlet Metal Angle [deg]	17.32	22.39	37.65	39.85
Mean diameter [m]	0.84	0.83	0.82	0.81
Mean Diameter to Blade Height Ratio	13.77	11.4	14.72	11.61
Rotor Inlet Temperature [K]	-	1473	-	1248
AN^2 [(RPM $\times$ m)^2]	8.708×10^6	1.343×10^7	1.552×10^7	1.197×10^7
Exit Mach Number	0.28	0.85	0.53	0.84
Stage Pressure Ratio	1.98		1.79	
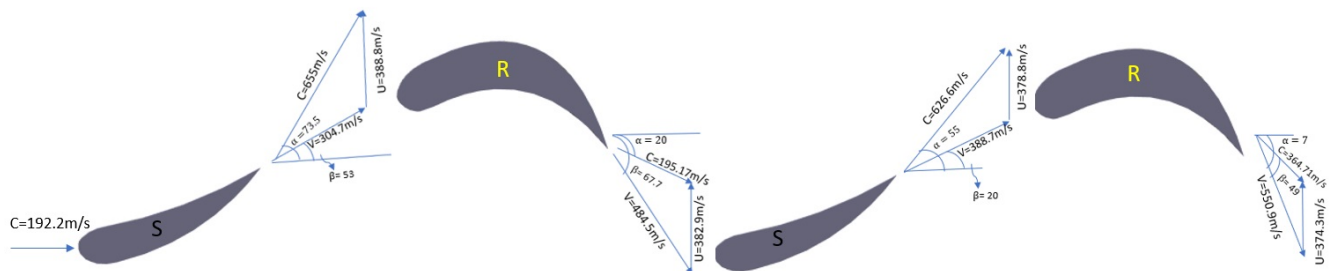
Figure 5.3: HPT Velocity Triangles

5.3 Low-Pressure Turbine

METU-PHOENIX features two stages uncooled Low-Pressure Turbine (LPT). According to the cycle analysis at the design point 13.5 Mega Watts of power at a mass flow of about 58 kg/s was needed. On the other hand, the LPT is limited by the max diameter of 0.99 meter so that it does not interface with bypass duct. Table 5.2 represents and compares the boundary conditions that was retrieved from GasTurb and the values that are achieved using AxSTREAM for the designed LPT.

5.3.1 LPT Design Results

Details of design parameters which has been obtained from AxSTREAM are given in Table 5.4 . When each parameter is compared with its typical values, it is seen that the results are consistent with the values stated previously in the turbine design guideline, Table 5.1.

Table 5.4: Detailed Design Parameters of Low Pressure Turbine

Variables	Stage 1		Stage 2	
	Stator	Rotor	Stator	Rotor
Flow Coefficient	1.05		0.65	
Stage Loading	1.24		2.47	
Degree of Reaction	0.82		0.55	
Power Extracted [MW]	4.39		8.28	
Isentropic Efficiency	0.91		0.89	
Zweifel Coefficient	0.67	0.68	0.85	0.62
Aspect Ratio	1.61	2.53	3.23	4.85
Solidity	1.34	1.43	1.34	1.43
Number of Blades	89	75	80	68
Stagger Angle [deg.]	0	63.93	17.22	30.07
Inlet Metal Angle [deg.]	65.69	133.53	38.06	49.58
Outlet Metal Angle [deg.]	90	24.18	22.79	18.42
Mean diameter [m]	0.94	0.94	0.94	0.94
Mean Diameter to Blade Height Ratio	10.94	7.8	4.96	3.66
Rotor Inlet Temperature [K]	-	1095	-	968
AN^2 [(rpm*m)^2]	6.22×10^6	6.53×10^6	9.12×10^6	7.06×10^6
Exit Mach Number	0.38	0.66	0.46	0.65
Stage Pressure Ratio	1.32		1.77	
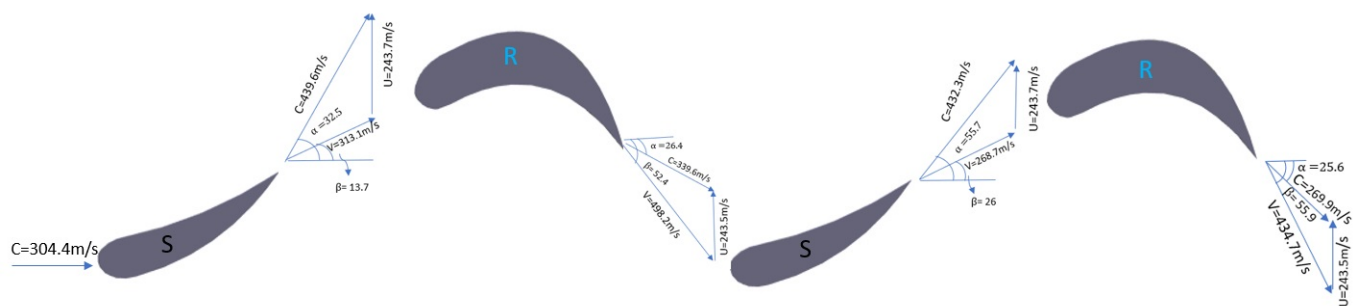
Figure 5.4: LPT Velocity Triangles

5.4 Turbine Off-Design Performance

It is critical to perform an analysis on off design performance of turbine.Turbine maps are generated and scaled using off-design option of GasTurb. As it can be seen in Figure 5.5, the HPT operates at 100% corrected speed at take off condition. Following figures show the turbine map for the HPT and LPT at take-off condition.
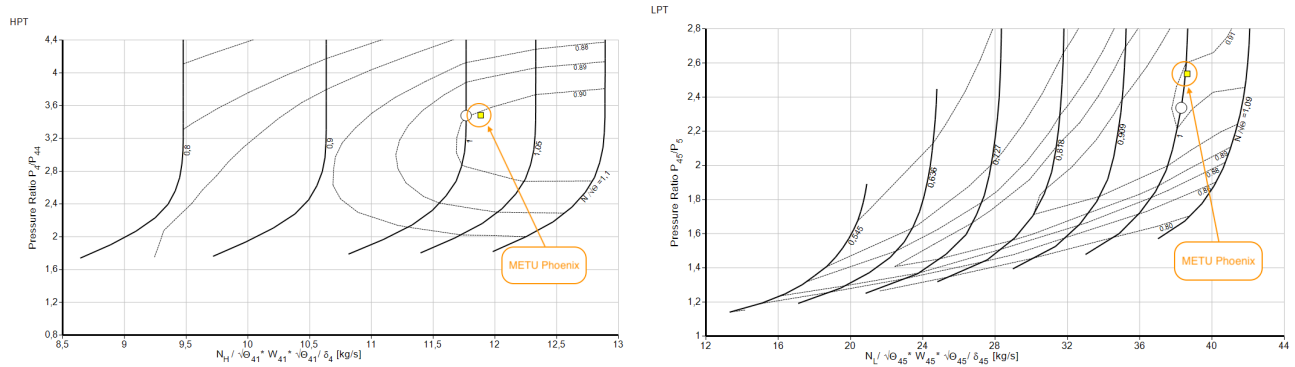
Figure 5.5: Off-Design Turbine Maps: HPT(Left) , LPT (Right)

5.5 Turbine Blade Cooling System

It is desired to have high turbine entry temperature at modern gas turbine engines as it can make the engine more compact and enhance the overall efficiency and performance of the engine. However, operating under extreme temperatures may lead to reduction of life time of turbine blades. Although the allowable temperature level of turbine blades are limited by the melting point of utilized material, blade cooling is necessary to drop the temperature of turbine blades to an acceptable level.

Therefore, number of different cooling techniques are considered for HPT blades. Thanks to recent advance manufacturing methods such as 3D printing of metals, building blades with multiple hollow passages has become much easier; as a result, a convection cooling is considered as it works mainly with the colder air taken from high pressure compressor (HPC) using air bleed channels; additionally, film cooling is considered such that number of holes on the body of blade airfoil are made for allowing coolant to pass from inner cavity to the outer surface throwing the refrigerant.
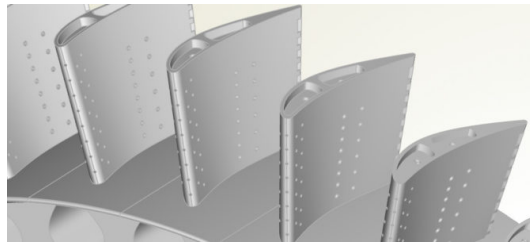
Figure 5.6: Hollow Passages on Turbine Blades

5.6 Smith Chart

In order to validate and analyze the efficiency of HPT and LPT, the aerodynamic coefficients.i.e. Average Flow Coefficient and Average Stage Loading Coefficients were retrieved from AxSTREAM and plotted on a general smith chart. It can be seen that HPT and LPT has an isentropic efficiency of about 93 and 91 , respectively.By comparing these the efficiency values that has been obtained from GasTurb, AxSTREAM and Smith chart, a strong consistency can be observed in terms of efficiency values.
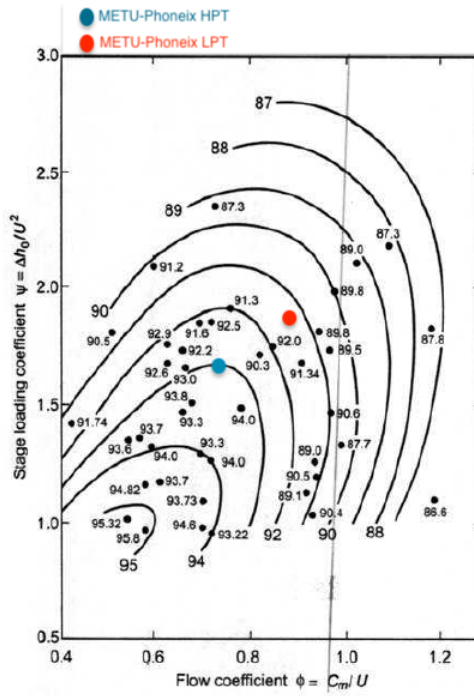
Figure 5.7: Smith Chart

5.7 Material and Manufacturing

Turbine is one of the hottest spots at any aero-engine; therefore, turbine blades undergo an immense amount of stress under very high temperatures. Selection of material for the turbine is made in a similar approach of compressor material selection. Results of turbine blade stress analysis can be found in the table below.

Table 5.5: Turbine Stress Analysis

Variables	HPT		LPT	
	Stage 1	Stage 2	Stage 1	Stage 2
Required Material Strength to Density Ratio	2.777×10^4	2.448×10^4	1.415×10^4	1.519×10^4
AN2 Rule [(RPM × m)^2]	8.708×10^6	1.552×10^7	6.538×10^6	7.06×10^6
Maximum Temperature [K]	1720	1473	1100	985

Analyzing information in Table 5.5, enabled the team to make a decision on turbine blade material. METU-PHOENIX engine will utilize CMC as the turbine blade material. CMC has a lower density in compare with conventional nickel super-alloy that is being widely used in industry. Additionally, CMC can provide longer lifetime under extreme high temperatures which is the case for the turbine. Information about CMC material can be found in the Table 4.10.

Due to the small size of turbine blades and necessity of having minute holes for cooling techniques, HPT blades, the SiC fibers must be manufactured using 3D printers and then electron beam drilling (EBD) to create small outer cooling holes.

LPT blades are uncooled with slightly larger blades, thus, they can be produced using traditional methods and cut using laser microjet.

6. MIXER

Mixer is significant in the aspect of mixing hot core flow and cold bypass flow to increase mixing efficiency and increase the gross thrust about a couple of percent and as a consequence lowering TSFC value [4].Mixer also contributes to noise reduction by lowering exit velocity, to mixer life extension by lowering the temperature and to stall margin increment.

6.1 Design Approach

Having lobed mixer provides faster mixing with small vortices.Mixer lobe peak direct exhaust gas radially outward toward the nacelle and mixer lobe valleys direct bypass air radially inward toward the centerbody.Also, mixer lobe valleys direct at least a portion of bypass air directly on the centerbody to increase the mixing efficiency. Aerodynamic shape of the lobes which are smaller and have more streamlined and less frontal area is minimizing drag, reducing pressure drop and create more uniform exit temperature. Moreover, they minimize axial vortex generation and angular momentum which also decrease the pressure loss.On the other hand, determination of the mixer lobe number is important. According to the study in [27], as the number of lobes increases mixedness index increases proportionally that is why lobe number is selected as 18. Moreover, increase mixing efficiency with minimum pressure loss, extending lobe channels toward the core region and zig-zag nails at the lobe tops are added.
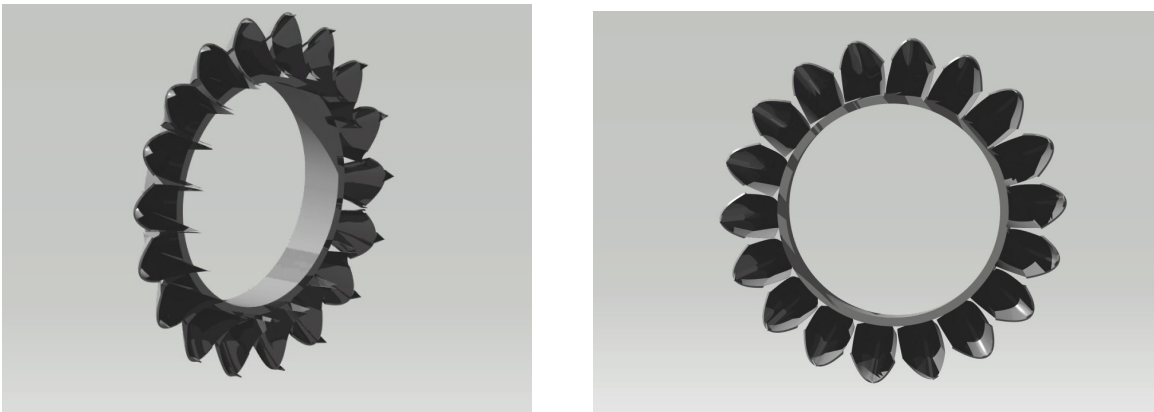
Figure 6.1: METU-PHOENIX Isometric (Left)and Front(Right) View of Mixer

6.2 Material and Manufacturing

Mixer section is important to increase the thrust produced by engine and to decrease the component noise which is known as the jet noise.Since noise is an major parameter in Concorde aircraft, METU-PHOENIX team payed an immense attention on the material selection of mixer and nozzle. Therefore, to reduce the overall engine noise level, noise absorbent materials are used for the mixer. Absorbent materials are selected to dissipate the higher frequency noise associated with the flowing fan air. For the METU-PHOENIX engine, N155 is selected as a mixer material.

Table 6.1: N 155 Properties

Parameter	Value
Maximum Service Temperature [K]	1144
Density [kg/m^3]	8249
Tensile Strength [MPa]	262
Young Modulus [GPa]	143

7.   EXHAUST SYSTEM

A well-designed exhaust system is critical to achieving a low-noise engine.The nozzle should also experience an ideal expansion while generating low drag.For this reason, significant attention is paid to the design and optimization of METU-PHOENIX's nozzle.

7.1   Nozzle Inlet Conditions

The inlet conditions for the nozzle are given in Table 7.1. These values are obtained from performance calculation carried on GasTurb.

Table 7.1: Nozzle inlet conditions.

M_{in}	T_{in} [K]	p_{in} [kPa]	D_{in} [m]	$\dot{m}$ [kg/s]
0.4	650.5	117.5	1.368	186.975

7.2   Nozzle Design Methodology

There are two types of nozzles, converging nozzle, and converging-diverging nozzle. It is suggested by [5] that if the ConDi nozzle generates at least 5% of thrust higher than the converging nozzle, then it should be definitely taken into consideration. The Equation 7.1 is used to help in making the decision.

$$\frac{F_{g-CD}}{F_{g-Conv.}} = \sqrt{\frac{1 - NPR^{-\frac{\gamma-1}{\gamma}}}{\frac{\gamma-1}{\gamma+1}} \frac{\gamma}{\gamma + \left(1 - \left(\frac{\gamma+1}{2}\right)^{\frac{\gamma}{\gamma-1}}.NPR^{-1}\right)}} \tag{7.1}$$

Knowing that NPR is 14.85, and assuming ideal expansion, Equation 7.1 is used to compute percent thrust gain and found to be 10.5%, which clearly shows that ConDi nozzle is the nozzle type to be designed for the METU-PHOENIX engine. Another design goal is that the nozzle is a fully variable one to achieve ideal expansion at different altitudes and Mach numbers.Method of Characteristics is an effective tool to design a nozzle with isentropic behavior or close to it, which is expected to have better noise performance [5].

Therefore, the method of Characteristics is applied for this design. A GUI (Graphical User Interface) is built by the METU-PHOENIX team where the algorithm is implemented to make the iterative design process more efficient.

This algorithm uses some empirical equations as well; these equations are needed to estimate the boundary layer development. Adding this to the algorithm is crucial to measure the nozzle's performance accurately because the losses inside the nozzle are due to the accelerated turbulent flow and its influence on the development of the boundary layer [28].

Starting with the exit Mach number, mas flow rate is known, which is $\dot{m} = 186.975 kg/s$, assuming that the flow is ideally expanded and the mass flow rate of the fuel is neglected. The difference between the exit velocity and free stream velocity is determined by applying Equation 7.2.

$$F = \dot{m}\Delta V \tag{7.2}$$

The thrust needed in cruise is 44.62 kN; hence, the exit velocity is measured to be 239 m/s higher than the free stream velocity. This value will be used to check the results obtained in the following parts.

The exit area is calculated using the Area-Mach relation given in Equation 7.3 to compare isentropic result with the one obtained by the method of characteristics to make sure that the outputs are determined correctly.

$$\left(\frac{A}{A*}\right)^2 = \frac{1}{M^2}\left[\frac{2}{\gamma+1}\left(1 + \frac{\gamma-1}{2})M^2\right]^{(\gamma+1)/(\gamma-1)} \tag{7.3}$$

Next, Figure 7.1 is used to find the adiabatic efficiency of the nozzle
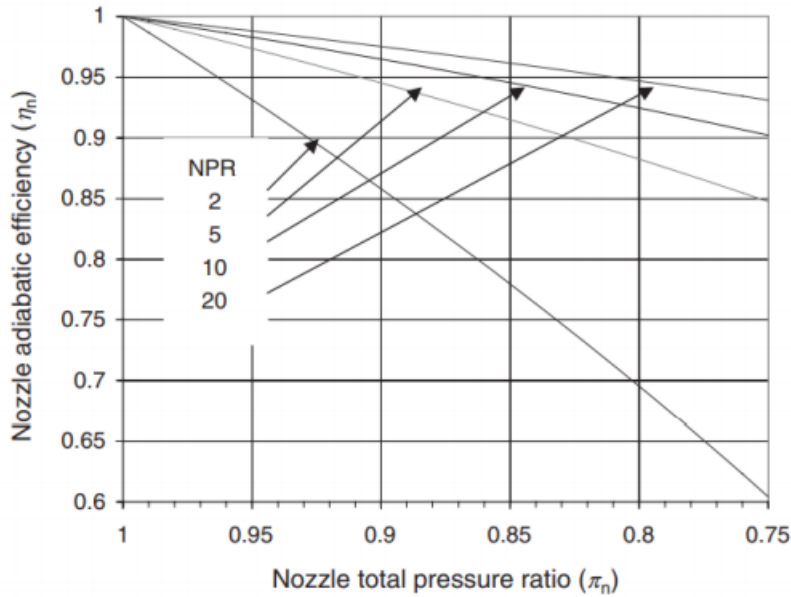
Figure 7.1: Nozzle adiabatic efficiency
[5]

7.3   Nozzle Performance

Now, GUI is used to get the result of the nozzle design. The exit Mach number rises slowly to expand the flow ideally. When the ideal expansion is developed, the mesh is then increased so that the output is more accurate. For example, results of the mesh density of 50 are shown in Figure 7.2.
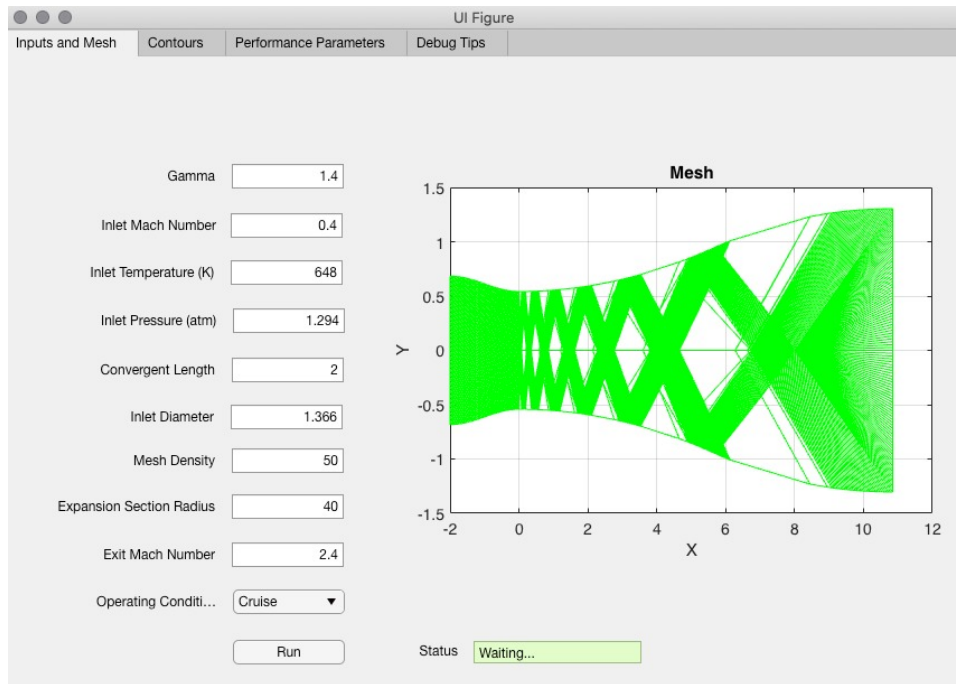
Figure 7.2: The inlet conditions and the characteristic mesh.

As shown in Figure 7.2, the characteristic mesh is successfully created. The exit Mach number is set to 2.4 while the expansion section radius is set to the lowest possible value. These ensure that the flow is ideally expanded with minimum exit area.
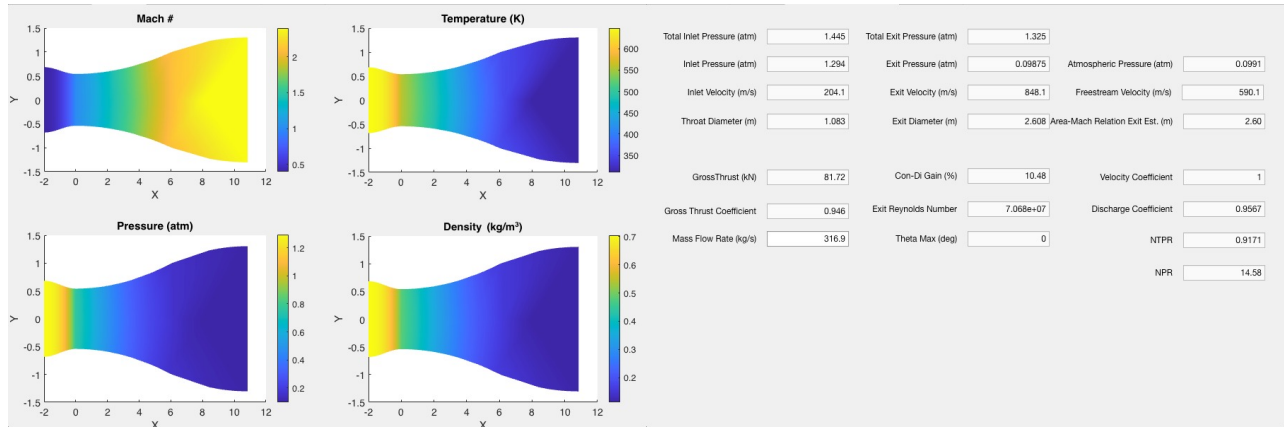
(a) Evolution of the aerodynamic properties.   **(b)** Performance parameters.

Figure 7.3: Nozzle performance obtained using Method of Characteristics.

It can be seen from the results that the difference between the exit velocity and the free stream velocity is 258 m/s which satisfies the value mentioned before, 239 m/s. It can also be seen that the exit pressure and the atmospheric pressure are the same. Finally, the thrust needed during the cruise is calculated.

CFD was conducted for validation of the accuracy of the 2D nozzle design. Information on 2D Nozzle CFD is provided in Table 7.2.

Table 7.2: 2D Nozzle CFD Properties

Mesh Program	ICEM CFD	**Yplus is below 1 along the nozzle wall**	
Mesh Technique	Block Mesh		
Solver		**Boundary Conditions**	
Program	Fluent	**Inlet**	Pressure Far Field Gauge Pressure: 117497 [Pa] Temperature= 650 [K] Mach Number =0.4
Type	Density-based	**Outlet**	Pressure Far Field Gauge Pressure: 10040 [Pa] Temperature= 217 [K] Mach number = 2.4
Time	Steady	**Nozzle**	Wall
2D Space	Planar	**Materials**	
Models		**Fluid**	Air
Energy	on	**Density**	Ideal-gas
Viscous Model	k-omega , SST	**Viscosity**	Sutherland

(a) Mach Contour of 2D Nozzle from CFD   **(b)** Temperature Contour of 2D Nozzle from CFD

Figure 7.4: Nozzle Mach Number and Temperature Contour using CFD.

38

As it can be seen in Figure 7.4, inlet and outlet thermodynamic properties (pressure, temperature, mach number, etc.) values of GasTurb and GUI created by the team agree on with each other; therefore, it can be concluded that there is a strong consistency between GasTurb, GUI and CFD results. Additionally, the shock diamonds have been appeared at the exit of the nozzle as it was expected and this means that the team's CFD results well predicted the existence of shock diamonds.

The nozzle looks lengthy because GUI applies the method of characteristics in 2D; however, the actual nozzle is less than that because of the 3D effects.

The exit diameter is found using both method of characteristics and Equation 7.3, the results of both ways are observed to be close to each other. That means, in order to have an ideal expansion in the nozzle, the exit area should be around $A_{exit} \approx 2.214 \; m^2$. However, it is not possible to get ideal expansion with a fixed diameter at all points in flight envelope. Figure 7.5 demonstrates the way that gross thrust coefficient varies for different throat to exit area ratios and NPR values.Figure 7.5 is used in order to validate the accuracy of the results once more.
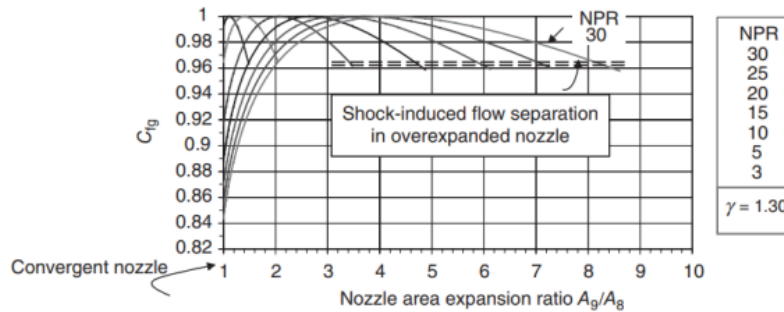
Figure 7.5: Gross thrust coefficient for different NPR and area ratios [5]

The maximum gross thrust coefficient for NPR = 14.58 when the exit to throat area ratio is approximately 2.6. It is clearly shown that the results of MATLAB GUI and Figure 7.5 are consistent with each other. Nozzle exit diameter is limited to the 0.839 m for the given throat diameter to prevent over-expansion. In actual operation, the characteristic lines is not going to reflect from the wall thus, the nozzle's performance will remain the same even when the deflection angle increase.

The performance parameters of the nozzle are given in Table 7.3.

Table 7.3: Performance of the METU-PHOENIX nozzle at cruise conditions.

Condition	C_D	π_n	NPR	η_n	C_{fg}
$M_\infty = 2.0$	0.9567	0.9171	14.58	0.96	0.946

The sizing of the nozzle including suppression channels is in Figure 7.6. The importance and effects of the suppression channels will be discussed later on.
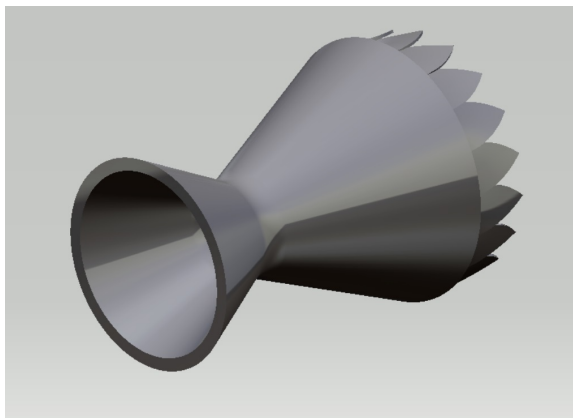
(a) METU-PHOENIX Isometric view of Nozzle
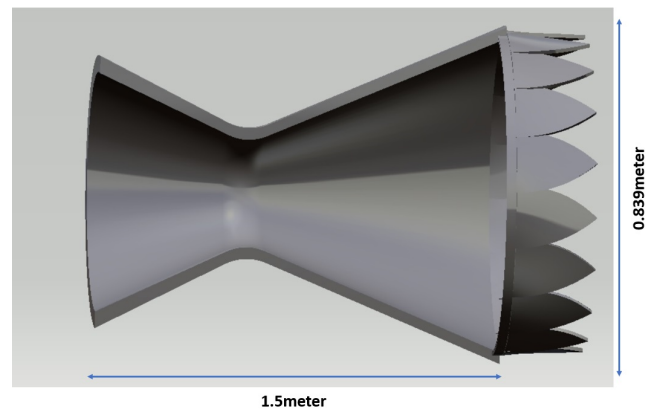
(b) METU-PHOENIX Side View of Nozzle

Figure 7.6: Nozzle Sizing

39

7.4 Chevron

To reduce the noise made by the engine, fixed chevrons are used at the trailing edge of the nozzle. Chevrons provide reduction in noise amount by dropping the jet exhaust velocity while keeping the engine cycle the same [29]. A nozzle without chevrons creates a large scale of secondary vortices that displace the overall jet downward and create a relative trajectory between the core and fan streams resulting increment of turbulence kinetic energy as it is described in the study of [30]. On the other hand, axisymmetric geometry of chevrons change the exhaust jet direction and decrease the formation of these vortices, resulting in a reduction in the noise created by the exhaust velocity. The same number of chevrons is used with the mixer's lobe number.

7.5 Material and Manufacturing

The METU-PHOENIX nozzle will be made out of N155. This material may have higher density in compare with its competitors; however, due to its noise frequency absorption capabilities which is an important parameter on this engine, the team decided to scarify the weight of engine a bit in order to satisfy the noise regulation requirements. This material has been used in F-16 at the early 2015 and it can be considered as a quite mature material. The information for N155 can be found in Table 6.1.

8.   AIRWORTHINESS AND ENGINE SUBSYSTEMS

8.1 Anti-Icing System

Prevention of the ice formation at the inlet is vital to not cause performance decrements and not to damage or disturb the engine components. Additionally, ice on fan blades produces imbalance which can cause vibration [31]. According to FAA Code of Federal Regulations Airworthiness Standards for Aircraft Engines (14 CFR Part 33) in section 77 [32], ice formation should not lead unacceptable power or thrust loss or engine to be shut down. Also used protection method must not obstruct the flow induction air into the engine much.

That is why, hydrophobic coating is applied to the inlet and the fan casing. Electrical system is connected to the inlet to keep temperature higher than the critical temperature value which varies with respect to local static pressure.

8.2 Fire Protection

According to FAA 14 CFR Part 33.17 [33], the engine must minimize the risk of fire spread in order to minimize probability of structural failure and hazardous effects.

By taking this into the consideration, the materials discussed in the previous chapters are chosen to minimize the probability of spread of the fire. Firewall is used to separate engine comportment from the cabin area. So in the case of fire, quantity of liquid, gas or flame do not spread to the other compartments of the aircraft. [34].

8.3 Secondary Power System

A secondary power system increases the power quality in the fixed frequency systems which contains Auxiliary Power System (APS) and Emergency Power System (EPS) [35].

Auxiliary Power System (APS) ensures main engine self-start capability, power to drive the main aircraft accessories for instance hydraulic pumps electric generators and emergency electric power to the Emergency Power System (EPS) by using a shaft driven electric generator (BSG) and compressed air for the Environmental Control System (ECS). Auxiliary power system (APS) of METU-PHOENIX engine is a combination

of an Auxiliary Power System (APS), an Electronic Starter Controller (ESC), an Air Turbine Starter (ATS), an Airframe Mounted Accessory Drive (AMAD), an Electronic Control Unit (ECU), a Brushless Generator (BSG), flow control valve and airframe mounted accessory drive. The working procedure of this system is APU's pneumatic power is converted to APU's shaft power while compressed air is supplied from APU to ATS. At the next step, ATS transmits air to AMAD. In order to start main engine and AMAD-mounted accessories, shaft power is transferred to the power take-off shaft. Additionally, Auxiliary Power System helps to decrease the fuel consumption and noise [35].

In the case of shutdown or any other unexpected situation, emergency power system (EPS) is used to maintain the systems work at their normal states. It contains thermal batteries, electrically driven hydraulic pump and inverter. These components generate power hydraulic and electrically. As a source of power, Auxiliary power Unit(APU)'s shaft power is used. This power is stored in the thermal batteries.The Inverter converts DC power to AC power when it is required [35].

8.4   Engine Control Systems

Full Authority Digital Electronic Engine Control (FADEC) system is used as engine control system in METU-PHOENIX just as Olympus 593 to increase communication with the engine, fuel efficiency, protection, reliability, maintenance and safety while reducing the pilot's workload. It ensures engine works properly without exceeding engine limits and damaging the components [36].

System is mounted on the engine, it provides reduction in electrical cable turn, weight, vibration and electrical interference. Cooling is achieved by fuel circulation to meet the required thermal conditions.

The brain of the FADEC system Engine Control Unit (ECU), receives and analyses the input of the flight condition such as air density, engine temperature, engine pressure etc. and compute engine operating parameters for instance fuel flow, air bleed vane position etc. from engine start to shut down with full authority. Since ECU performs signal conditioning, computation and output signal processing, its properties are important. Its structure is based on dual- lane configuration also inter-lane communication and duplicated computers with comparison monitoring enables ECU to have high degree of fault detection and safety abilities [36] [37]. Electrical power is obtained by the accessory mounted on the engine. The unit communicates with the aircraft by the fiber optic cables.

Operating principle is shown in Figure 8.1, input of ECU is a combination of operating conditions determined by sensors and control instructions from the flight crew. Instruction output module convert control signal suitable to actuators. Converted signals are received by engine's relevant part and engine functions are adopted.

Figure 8.1: Block Diagram of the FADEC
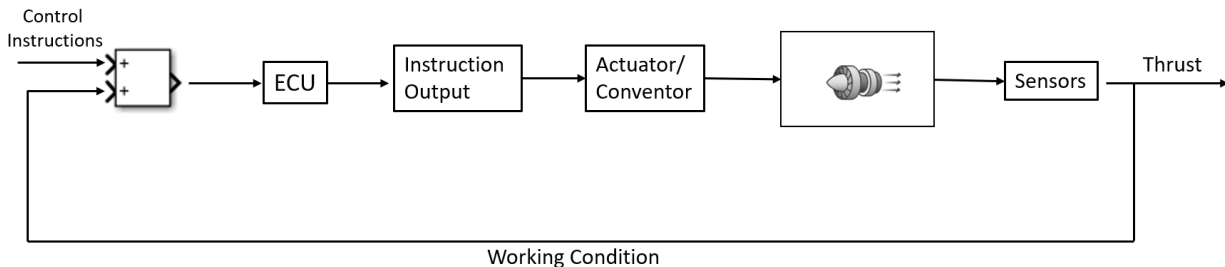
8.5 Fuel System

According to FAA 14 CFR Part 33.67 [38], for an amount of fuel supplied to the engine at the specified flow and pressure, engine must function properly. Fuel filters have to be used between the engine fuel inlet opening and the inlet of the fuel metering device.

In METU-PHOENIX, signals received from FADEC system control the fuel system. Fuel is taken from the tanks, pressurized and injected into the combustion chamber. Fuel filters are used for ensuring the necessary protection of the engine fuel system against the foreign particles. It is easily removable and accessible for maintanence purposes.

8.6 Lubrication System

Lubrication system is vital to improve energy efficiency by reducing friction and increase service life of the rotating parts. Also, it reduces engine operating temperature. Lubrication system mainly consists of oil tanks, oil pressure pump, supply lines, scavenge pump, return lines, filters, oil coolers. According to FAA 14 CFR Part 33.71 [39], lubrication system must function properly in different flight attitudes and atmospheric conditions. Suitable oil filters should be used to protect oil system. Oil tank must be vented from the top part to avoid any water vapor accumulation in the lines and oil tank must have oil quantity indicator.

MIL-PRF-236999 HTS is selected as a lubricant [40] for METU-PHOENIX, since its viscosity and high temperature stability is superior. For the system, additive usage is important to enable main lubricant to gain additional properties and characteristics. Boundary lubrication, antioxidants, anti-corrosion, anti-foaming additives are determined to be used in the system.

For having larger oil capacity and to control the oil temperature, METU-PHOENIX utilize dry-sump lubrication system to cool down compressor and turbine bearings. This contains oil tank pump, piping, filters and oil cooler.

To maintain oil temperature, oil cooling is important.Cooling is achieved by fuel supply.Fuel acts as a heat exchanger, as a result, oil transfer its high temperature to the fuel.

8.7 Noise-Reduction Review

Though aircraft is the leading cause of noise at the airport, engine noise is considered one of the significant contributors to the overall noise caused by the aircraft [29]. Turbofan engines help to reduce the noise caused by the exit velocity, thanks to their bypass air.

Technologies are being studied to reduce the noises caused by the engines. METU-PHOENIX uses some of those technologies by adjusting the engine cycle parameters and using low-noise design features to ensure a reduction in engine noise. As mentioned in detail, the low-noise design features were considered when deciding on the mixer geometry and the choice of chevron configuration in the nozzle.

Chevron nozzles are considered one of the best low-noise design features since they have been tested by NASA in 1996 [29]. Chevron nozzles reduce the jet noise by around 2.5 EPNdB without having changes in the engine cycle. Thus, the noise caused by the engine will be reduced more after applying changes in the engine cycle which gives an advantage to METU-PHOENIX.

For the preliminary design phase of METU-PHOENIX, the noise analysis considered the changes in the engine cycle, the use of noise-absorbing material, secondary power system, optimization of the mixer's geometry, and the use of chevron nozzles. In the future phases of the design, further low-noise design features will be considered to reduce the engine noise more. These features include the study of different noise-absorbing materials, active-noise control devices, and the adjustment in the turbomachinery blades, especially for the tip velocities.

9. PERFORMANCE CONSTRAINT ANALYSIS

9.1 Drag Polar Estimation

Drag polar estimation is required for constraint and weight analysis. Table 9.1 shows the estimations done for different flight configuration such as clean, take-off gear up, take-off gear down, landing gear up ,landing gear down. These relations are obtained according to the method described in [10].

Table 9.1: Drag Polar Estimation for METU-PHOENIX

Flight Configuration	Drag Polar Estimation
Clean	$0.0126 + 0.22C_L^2$
Take-off Gear Up	$0.0276 + 0.23C_L^2$
Take-off Gear Down	$0.0476 + 0.23C_L^2$
Landing Gear Up	$0.0776 + 0.25C_L^2$
Landing Gear Down	$0.0976 + 0.25C_L^2$

9.2 Performance Constraint

Table 9.2: Constraints for METU-PHOENIX[10]

Constraint	Constraint Relation	Parameters
Takeoff Distance	$(T/W)_{TO} = \frac{4(4+\lambda)}{3(5+\lambda)} + \frac{\frac{0.0447(W/S)_{to}}{s_{tog}\rho} + 0.721C_{DO}}{C_{LmaxTO}} + \mu$	Bypass ratio at take-off$(\lambda)is2$, Runway length (s_{tog}) is 2286 m, density at standard sea level conditions Drag polar coefficient (CDO) is taken at takeoff gear down condition, Ground friction coefficient for asphalt (μ) is 0.03 $1.2 < C_{Lmax} < 1.8$
Landing Distance	$W/S = \frac{\rho \cdot V_{SL}^2 C_{Lmax,L}}{2\frac{W_L}{W_{TO}}}$	Landing stall speed (V_{SL}) is 45.7 m/s due to FAR regulations, Landing weight to takeoff weight$(\frac{W_L}{W_{TO}}) = 0.75$ for supersonic jet transportation [10] $1.8 < C_{Lmax,L} < 2.2$.
Supersonic Cruise (M=2)	$(T/W)_{TO} = \frac{\beta}{\alpha}(K1\frac{\beta}{q}(\frac{W}{S})_{to} + \frac{CD0}{\frac{\beta}{q}(\frac{W}{S})_{to}}$	Thrust ratio (α) calculated as 0.2976 Weight ratio (β)estimated as 0.95, Dynamic pressure at cruise conditions CD0 is for clean condition. Viscous drag coefficient (K1) is a function of $C_{Lmax,C}$. $1.2 < C_{Lmax,C} < 1.8$
Climb	$T/W = \frac{N}{N-1}(\frac{1}{1/L/D} + CGR)$	Number of engines(N) are 4, Climb gradient(CGR) is 0.027 according to FAR 25.121. [10]. L/D is taken according to RFP.

Determination of constraints are significant for the aspect of finding the critical W/S and T/W values which are important to meet the performance requirements. According to [10] for the supersonic transport, the con-

straint relations for take-off distance, landing distance, supersonic cruise and climb are given in the Table 9.2 respectively. These relations are generated according to the FAR 25.121 (supersonic jet transport) regulations.

Figure 9.1: T/W vs W/S Graph According to the Constraints
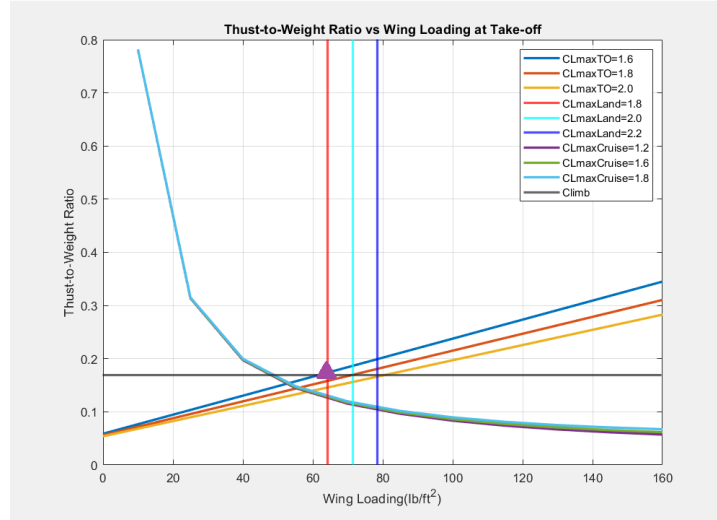
Purple triangle on the Figure 9.1 indicates T/W is 0.2 and W/S is 317 kg/m^2 at the operating design point for Concorde with METU-PHOENIX engine.

10. WEIGHT ANALYSIS

10.1 Weight of the METU-PHOENIX Components

According to RFP, weight of the Olympus 593 engine is given as 3175 kg without inlet, nozzle, tailpipe and casing and general categories of the used materials for each components are provided. While doing performance calculations in Gasturb 13 for METU-PHOENIX, based on provided information, weight of each component is calculated as it shown in the 2nd column of the Table 10.1. However, with the improvements and the innovations in the material science and technology over the years, it is possible to decrease the total weight of the METU-PHOENIX. In previous chapters, the materials chosen for each component is defined with this reason as well. The density of the selected materials and Gasturb data for each component geometry are used for estimation of the METU-PHOENIX engine's actual weight as it shown in 3rd column of the Table 10.1. As a result, by using advanced materials, METU-PHOENIX engine weight without inlet, nozzle, tailpipe and casings,is 1495 kg less than Olympus 593. The component based weight comparison according to the material is provided in Table 10.1.

Table 10.1: Weight Comparison of METU-PHOENIX Components with Different Materials

Component	METU-PHOENIX Weight with Olympus 593 Materials [kg]	METU-PHOENIX Weight with Selected Materials [kg]
Fan	1545	560
HPC	480	546
CC	129	41
HPT	121	32
LPT	393	103
Mixer	79	166
Bypass Duct	196	79
LP Shaft	26	25
HP Shaft	25	25
Exhaust	106	104
Total	3100	1680

10.2 Mission Weights

As it is mentioned, METU-PHOENIX engine's weight is significantly less than Olympus 593. According to RFP, Maximum Take-off Weight (MTOW) can be calculated for Concorde as 185,000 kg. Furthermore, by subtracting the engine weight difference for 4 engines, new MTOW is calculated as 179,020 kg for Concorde with METU-PHOENIX engine. This value is used for weight fraction calculations to make fuel usage estimation. Also 0.4 hours loiter is added to the mission to ensure engine can operate in an emergency or unexpected situation at $M = 0.5$ and 4,572 m altitude. Table 10.2 describes the weight fraction relations for supersonic jet transportation [20].

In following table unknown TSFC values are estimated with the $TSFC = (C_1 + C_2 M)\sqrt{\theta}$ relation where $C_1 = 0.45$ and $C_2 = 0.54$ for turbofan engines. Thrust-to-weight ratio, wing loading and drag coefficient (at takeoff gear down, at climb, cruise and loiter clean, and at landing gear up configuration are all considered) values are determined from the constraint analysis chapter. Thrust ratio (α) and weight ratio (β) takes different value for each mission segment. Dimensionless static temperature ratio of atmosphere depend on the altitude and the values are obtained from the appendix in [20]. The cruise range from Paris to NewYork, duration of the mission segment, sound of velocity at sea level condition, ground coefficient, dynamic pressure at mission speed and altitude are denoted by $\Delta s, \Delta t, a_{std}, \mu_{TO}, q$ respectively.

Table 10.2: Weight Fraction Relations

Mission Segment	Weight Fraction Relation
Warm-up	$W_f/W_i = 1 - C_1\sqrt{\theta}\frac{\alpha}{\beta}(\frac{T_{SL}}{W_{TO}})\Delta t$
Taxi	$W_f/W_i = 1 - (C_1 + C_2 M_{TO})\sqrt{\theta}\frac{\alpha}{\beta}(\frac{T_{SL}}{W_{TO}})\Delta t$
Take-off	$W_f/W_i = e^{\left(-\frac{(C_1+C_2 M)\sqrt{\theta}}{g_0}\left(\frac{V_{TO}}{1-(C_{D_{TO}}(\frac{q}{\beta})(\frac{S}{W_{TO}})+\mu_{TO})\frac{\beta}{\alpha}\frac{W_{TO}}{T_{SL}}}\right)\right)}$
Subsonic- Transonic Climb/Descend and Landing	$W_f/W_i = e^{\left(-\frac{(C_1/M+C_2)}{a_{std}}\left(\frac{\Delta(h+V^2/2g_0)}{1-(\frac{C_D}{C_L})(\frac{\beta}{\alpha})\frac{W_{TO}}{T_{SL}}}\right)\right)}$
Cruise	$W_f/W_i = e^{\left(-\frac{(C_1/M+C_2)}{a_{std}}(\frac{C_D+C_{DR}}{C_L})\Delta s\right)}$
Loiter	$W_f/W_i = e^{\left(-(C_1+C_2 M)\sqrt{\theta}(\frac{C_D+C_{DR}}{C_L})\Delta t\right)}$

According to the described procedure, weight fractions and as a consequence total fuel usage estimation is obtained, shown in Table 10.3. Mission altitudes are determined according to RFP.

Table 10.3: Mission Segment Fuel Weight Analysis of the Concorde Operating with the METU-PHOENIX

Mission Segment	Start Height [m]	End Height [m]	Time [h]	Weight Left Guess [kg]	Fuel Usage Guess [kg]	Fuel Percent Usage [%]	TSFC [g/(kN*s)]	Weight Fraction
1)Warm-up/ Taxi	0	0	0.15	176610	2417	6.32	-	0.9865
2)Take-Off	0	9144	0.05	176300	2722	7.12	18.6	0.9848
3)Subsonic Climb	9144	12192	0.015	175000	1300	3.39	14.7	0.9926
4)Transonic Climb	12192	16154	0.015	174670	327	0.86	20.22	0.9981
5)Cruise	16154	16154	3	157210	23916	62.54	27.95	0.8631
6)Loiter*	4572	4572	0.4	150002	7187	18.79	14.7	0.9543
7)Descend/ Landing	16154	0	0.15	14800	374	0.98	-	0.9975
Total					38243			

11. COST ANALYSIS

11.1 Production Cost

Production cost includes the cost of direct and indirect labor cost, material cost, tooling, technical publications, testing, field service, profit and component improvements [41].The equations for cost estimation for aircraft turbine engine production for U.S. Airforce is given in [41]. The described method based on performance data and engine costs are given in dollars value in 1980 for various turbofan and turbojet engine costs. Equations are derived only as a function of engine performance parameters. For production cost estimation, they are maximum thrust, maximum Mach number and turbine entry temperature value. To provide more accurate comparison, production cost is estimated for the first METU-PHOENIX and dollars value in 1980 is converted to dollars value in 2021. Material cost is calculated based on material's (mentioned in the previous chapters) price per kg and shown in Table 11.1.

Table 11.1: Production Cost Estimation of METU-PHOENIX

Cost(Thousand Dollars)	Materials	Manufacturing,Labor, Testing,Management,Tooling, Publications Improvements	Production
METU-PHOENIX	217	8778	8995

11.2 Fuel Cost

Fuel price is highly depended on political, social and technological impacts. Service entry date for METU-PHOENIX engine is 2028 that is why fuel price estimation is done. For this purpose, previous and present fuel prices provided on EIA website for jet fuel [42] and jet fuel price estimation in AIAA Conference report [43] are used. In AIAA report price estimation is based on crude oil price and demand. For different rate of demand, estimations are done. Reference case for crude oil price is taken into account and the Figure 11.1a is obtained.
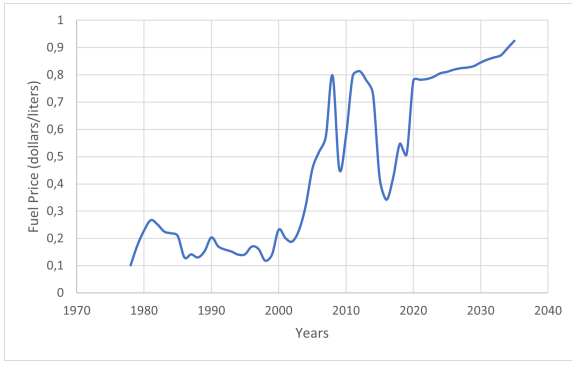
(a) Fuel Price Estimation for Service Entry Year
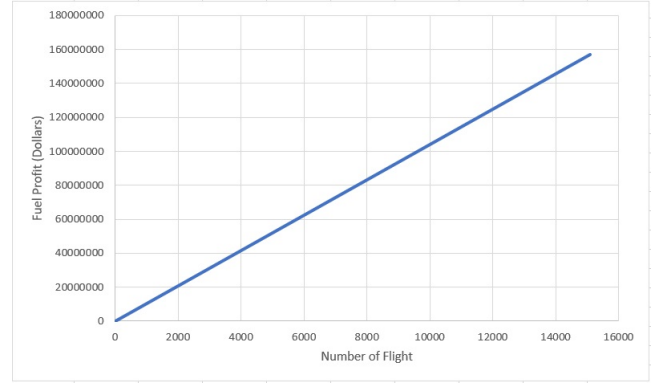
(b) METU-PHOENIX Fuel Profit per Number of Flights

Figure 11.1: Fuel Cost Estimation

According to the figure, in 2028 estimated fuel cost is 0.84 dollar/liters. In Chapter 10, total fuel weight is estimated as 38,243 kg which is equal to 47,566 lt according to Jet A1 fuel density. For Paris to Newyork flight, total fuel cost is estimated as $39,955$ for Concorde with 4 METU-PHOENIX engine. In METU-PHOENIX engine design, TSFC is reduced by 26% relative to Olympus 593 engine. This decreament introduces $10,388 profit per flight which is illustrated in 11.1b.

11.3   Maintenance Cost

Engine maintenance cost contains labor, material, fuel, oil costs and indirect maintenance costs such as controlling, monitoring, administrating, testing and tooling. After studied in ATA, NASA and AEA maintenance cost estimation methods which are based on various aircraft's parameters that operate at different speeds and ranges [44], results obtained from AEA methods are selected. It is more accurate and suitable for long range and high speed operating engines. To provide more accurate comparison, both Olympus 593 and METU-PHOENIX engine maintenance costs are estimated according to the method. Price given is converted to value of dollars in 2021. The comparison of the maintenance cost given in Figure 11.2. According to the AEA method, total maintenance cost is found from Equation 11.1.

$$C_{emm} = C_{em}C_{el}(\frac{t_f + 1.3}{t_f - 0.25}) + C_{bur} + C_{fuel} \tag{11.1}$$

Engine labor cost relation is found from Equation 11.2.

$$C_{el} = 0.21C_1C_3C_{lr}(1 + T_{eng})^{0.4} \tag{11.2}$$

Where $C_1 = 1.27 - 0.2(BPR)^{0.2}$ and $C_3 = 0.032$. C_{lr} represents the labor cost per hour which is taken as $25 and t_f is the flight time.
Engine material cost relation is given in Equation 11.3.

$$C_{em} = 2.56C_1(C_3 + C_2)(1 + T_{eng})^{0.8} \tag{11.3}$$

Where $C_2 = 0.4(\frac{OPR}{20})^{1.3} + 0.4$.
Maintenance burden, in other words indirect costs (C_{bur}) estimated as twice of the engine labor cost. Fuel cost C_{fuel} estimation is done in previous section. To get total maintenance cost, calculated fuel cost is also added. The comparison of maintenance cost between Olympus 593 and METU-PHOEIX engine can be seen in Figure 11.2.
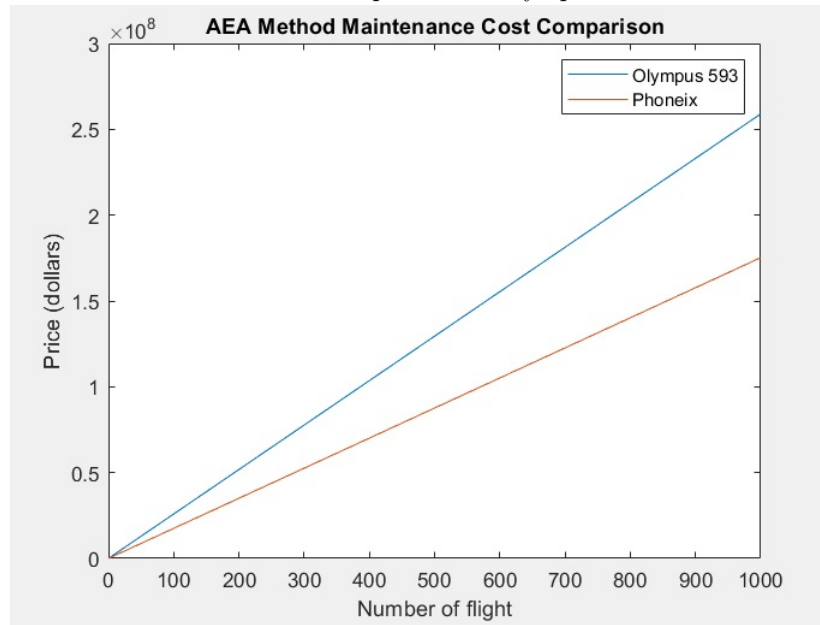
12.   Conclusion and Recommendation

In summary, METU-PHOENIX is a candidate engine to be installed on the Concorde. The engine allows the aircraft to cruise at Mach 2.0. The design of METU-PHOENIX began by setting the design goals of reduced SFC, weight, and noise without the usage of afterburner at take off. Furthermore, each major component of the flow path was developed with high performance and reliability in consideration.

In conclusion, METU-PHOENIX meets all the engine requirements besides the NOx emissions while reducing SFC by 26% and eliminating excessive jet noise. During design stage logical assumptions were made such that METU-PHONEIX engine's performance data would have a quite reasonable and reliable values. Also, weight is reduced by 47% (1,495 kg) in METU-PHONEIX with the innovations and improvements of the material science and improved performance parameters. This weight reduction and the improved SFC value introduces fuel weight decrements. Fuel weight is estimated as 38,243 kg, this provides $10,388 fuel cost profit per flight. Additionally, significant profit in maintenance cost is obtained according to the analysis.

Further studies will be conducted in the upcoming design phase to improve the performance of the engine. These studies will include optimization in the turbomachinery components and their off-design performance, noise estimation and reduction, shaft vibrations analyses and its related noise and losses. Moreover, if such a work of future development for the continuation of efforts is possible, designer team wish to carry the preliminary design to high fidelity computer programs to check the performance of the components.

Appendix

Cruise SI stations

	Units	St 2	St 21	St 25	St 3	St 4	St 44	St 45	St 5	St 6	St 13	St 16	St 64	St 8	St 9
Mass Flow	kg/s	185,785	57,3587	57,3587	55,5806	50,7476	56,8276	57,688	58,5484	58,5484	128,426	128,426	186,975	186,975	186,975
Total Temperature	K	398,833	469,738	469,738	899,917	1721,45	1279,25	1268,49	1053,35	1053,35	477,577	477,627	669,568	669,568	669,568
Static Temperature	K	376,988	447,843	447,843	893,701	1699,57	1240,83	1238,18	1013	1045,52	463,101	470,425	650,542	564,808	349,573
Total Pressure	kPa	75,0743	127,626	126,35	1175,05	1128,05	324,366	317,879	136,448	133,719	135,134	132,431	130,855	130,855	130,855
Static Pressure	kPa	61,6003	107,7	106,624	1143,96	1064,96	284,75	286,687	116,043	129,644	121,122	125,465	117,497	69,6621	12,4653
Velocity	m/s	209,905	211,441	211,441	117,472	237,815	307,038	272,667	309,955	136,545	171,929	121,271	202,013	472,242	816,705
Area	m²	1,55486	0,3238	0,327071	0,106103	0,097754	0,23151	0,262288	0,473322	0,992592	0,819815	1,13979	1,47098	0,921463	1,84293
Mach Number		0,54	0,5	0,5	0,2	0,3	0,45	0,4	0,5	0,217	0,4	0,28	0,4	1	2,18337
Density	kg/m³	0,569242	0,837787	0,829409	4,45925	2,18294	0,79946	0,806629	0,39908	0,431986	0,911148	0,929124	0,629212	0,429674	0,124225
Spec Heat @ T	J/(kg*K)	1013,4	1024,66	1024,66	1120,88	1290,19	1231,49	1229,1	1190,68	1190,68	1025,91	1025,92	1077,29	1077,29	1077,29
Spec Heat @ Ts	J/(kg*K)	1011,5	1021,15	1021,15	1119,5	1288,22	1225,47	1224,36	1182,57	1189,11	1023,6	1024,77	1072,6	1052,24	1015,37
Enthalpy @ T	J/kg	101528	173906	173906	634681	1,67104E6	1,10711E6	1,0934E6	832523	832523	181909	181960	385675	385675	385675
Enthalpy @ Ts	J/kg	79498,4	151552	151552	627781	1,64276E6	1,05998E6	1,05623E6	784487	823201	167129	174607	365270	274168	52171,3
Entropy Function @ T		1,02163	1,60345	1,60345	4,01708	6,91768	5,59023	5,55174	4,76625	4,76625	1,66231	1,66268	2,91326	2,91326	2,91326
Entropy Function @ Ts		0,823822	1,4337	1,4337	3,99026	6,86013	5,45997	5,44846	4,60428	4,73531	1,55284	1,60864	2,80559	2,28283	0,562127
Exergy	J/kg	175346	244466	243828	692920	1,54218E6	983403	970854	706142	704857	252362	251104	374500	374500	374500
Gas Constant	J/(kg*K)	287,05	287,05	287,05	287,05	287,046	287,047	287,047	287,047	287,047	287,05	287,05	287,049	287,049	287,049
Fuel-Air-Ratio		0	0	0	0	0,025193	0,022437	0,022095	0,021763	0,021763	0	0	6,7144E-3	6,7144E-3	6,7144E-3
Water-Air-Ratio		0	0	0	0	0	0	0	0	0	0	0	0	0	0
Inner Radius	m	0,197274	0,412092	0,229732	0,35945	0,401037	0,401037	0,401037	0,401037	0	0,527387	0,567096	0	0	0
Outer Radius	m	0,730646	0,522387	0,396089	0,403417	0,438117	0,484275	0,494287	0,558116	0,562096	0,730646	0,827286	0,684271	0,555651	0,785809
Axial Position	m	0,365323	0,365323	1,52877	2,39386	2,71561	2,78659	2,9069	3,21774	3,77585	1,24031	3,77585	4,60314	5,08213	5,86004

Take-off SI stations

	Units	St 2	St 21	St 25	St 3	St 4	St 44	St 45	St 5	St 6	St 13	St 16	St 64	St 8	St 9
Mass Flow	kg/s	357,123	124,513	124,513	120,653	110,239	123,438	123,438	127,173	127,173	232,611	232,611	359,784	359,784	359,784
Total Temperature	K	303,577	391,036	391,036	810,529	1669,29	1238,75	1238,75	998,945	998,945	398,802	398,846	624,039	624,039	624,039
Static Temperature	K	269,622	366,067	365,881	804,992	1646,91	1199,43	1208,31	948,24	989,634	388,889	393,867	606,286	525,508	525,508
Total Pressure	kPa	103,083	227,004	224,19	2433,7	2361,46	678,045	663,866	262,512	256,165	244,707	240,619	242,835	242,835	242,835
Static Pressure	kPa	68,0855	180,053	177,504	2370,01	2222,96	590,677	596,838	212,317	246,577	224,006	230,233	217,987	129,125	129,125
Velocity	m/s	261,088	224,414	225,249	110,869	239,825	310,781	273,491	344,448	147,605	141,397	100,218	195,271	456,13	456,13
Area	m²	1,55486	0,3238	0,327071	0,106103	0,097754	0,23151	0,262288	0,473322	0,992592	0,819815	1,13979	1,47098	0,921463	0,921463
Mach Number		0,793077	0,585767	0,588092	0,198274	0,30721	0,462983	0,406001	0,573268	0,240776	0,358218	0,252307	0,399869	1	0,999999
Density	kg/m³	0,879713	1,71349	1,69009	10,2565	4,70229	1,71562	1,72078	0,780037	0,86801	2,00667	2,03639	1,25256	0,856	0,856
Spec Heat @ T	J/(kg*K)	1005,11	1012,72	1012,72	1101,04	1286,86	1226,44	1226,44	1180,84	1180,84	1013,4	1013,4	1067,56	1067,56	1067,56
Spec Heat @ Ts	J/(kg*K)	1004,07	1010,55	1010,53	1099,81	1284,6	1220,24	1221,65	1169,5	1178,76	1012,53	1012,97	1063,16	1044,81	1044,81
Enthalpy @ T	J/kg	5463,63	93665,1	93665,1	535460	1,60562E6	1,05835E6	1,05835E6	768390	768390	101497	101542	337253	337253	337253
Enthalpy @ Ts	J/kg	-28619,8	68484,2	68296,7	529314	1,57686E6	1,01005E6	1,02095E6	709068	757497	91500,7	96520,1	318188	233226	233226
Entropy Function @ T		0,063248	0,9523	0,9523	3,61235	6,78635	5,45724	5,45724	4,54984	4,54984	1,02136	1,02175	2,65335	2,65335	2,65335
Entropy Function @ Ts		-0,351525	-0,720583	0,718798	3,58584	6,72591	5,31929	5,3508	4,33763	4,51169	0,932972	0,977631	2,54541	2,02175	2,02175
Exergy	J/kg	1523,02	81198,6	80130,8	498358	1,2943E6	753981	752172	460471	458376	89547	88116,2	184973	184973	184973
Gas Constant	J/(kg*K)	287,05	287,05	287,05	287,05	287,046	287,046	287,046	287,047	287,047	287,05	287,05	287,049	287,049	287,049
Fuel-Air-Ratio		0	0	0	0	0,025918	0,023083	0,023083	0,02239	0,02239	0	0	7,8013E-3	7,8013E-3	7,8013E-3
Water-Air-Ratio		0	0	0	0	0	0	0	0	0	0	0	0	0	0

Bibliography

[1] Arthur H. Lefebvre and Dilip R. Ballal. *Gas turbine combustion: alternative fuels and emissions.* 2010.

[2] Jack D. Mattingly, Keith M. Boyer, Brenda A. Haven, William H. Heiser, and David T. Pratt. *Aircraft engine design.* American Institute of Aeronautics and Astronautics, Inc, 2002.

[3] Mach 2 concorde magazine, October 2017.

[4] Fletcher P. Walsh P.P. *Gas Turbine Performance.* Blackwell Science, second edition, 2004.

[5] Saeed Farokhi. *Aircraft Propulsion.* John Wiley Sons, second edition, 2014.

[6] Mechanical properties of carbon fiber composite materials, fibre / epoxy resin (120°c cure).

[7] Cyptec Engineering Material, 2019.

[8] The online materials information resource.

[9] Fan Renyu and Zhang Man. Low emission commercial aircraft engine combustor development in china:from airworthiness requirements to combustor design, Nov 2011.

[10] J Roskam. *Aircraft Design: Preleminary Sizing of Airplane.* DARcorporation, 1985.

[11] *Lets Re-Engine the Concorde.*

[12] Ge successfully tests world's first rotating ceramic matrix composite material for next-gen combat engine.

[13] Ali Gülhan Andreas K. Flock. Experimental investiogation of the starting behaviour of a three-dimensional scramjet intake. September 2015.

[14] P.E. Rich DeFrancesco Eric Gamble, Dwain Terrell. Nozzle selection and design criteria. 2004.

[15] SUN-HO GO, SEONG-MIN YUN, HEE-JAE SHIN, JANG-HO LEE, LEE-KU KWAC, and HONG-GUN KIM. Mechanical properties of cfrp/eva composites according to lamination ratio. *International Journal of Mechanical Engineering*, 2, 2017.

[16] J. Jankovec. Optimization of turbine blade fir-tree root geometry utlizing ls-prepost in pre and post-processing, 2015.

[17] Robert R. Tacina. *Low NOx potential of gas turbine engines.* National Aeronautics and Space Administration, 1990.

[18] Editor@optimage.co.uk. 28th congress of the international council of the aeronautical sciences, 23 - 28 september 2012, brisbane, australia paper icas 2012-4.10.2.

[19] Mach 2. *Concorde Magazine*, Oct 2017.

[20] Jack D. Mattingly, Keith M. Boyer, Brenda A. Haven, William H. Heiser, and David T. Pratt. *Aircraft engine design.* American Institute of Aeronautics and Astronautics, Inc, 2018.

[21] Arthur H. Lefebvre. *Gas Turbine Combustion.* Hemisphere Publishing Corporation, 1983.

[22] A. Selweyn C. Priyant Mark. Design and analysis of annular combustion chamber of a low bypass turbofan engine in a jet trainer aircraft. *Propulsion and Power Research*, May 2016.

[23] Jerry M Seitzman. Common engine atomizers, 2017.

[24] Diego Bracho García. Ceramic matrix compositesmanufacturing and applications in the automotive industry.

[25] D. A. Sagerser, S. Lieblein, and R. Krebs. Empirical expressions for estimating length and weight of axial-flow components of vtol powerplants. 1971.

[26] R Denney. Turbine design guidelines., May 2020.

[27] Ergin Ç. C. İper B. Süer T.U. Uslu S. Cenik, B. Investigation of the effects of lobe number and configuration on mixing performance in lobed mixer. *AIAA Propulsion and Energy Forum*, 2020.

[28] D. Boldman and R. Graham. Heat transfer and thermal boundary layer in a conical nozzle. *5th Propulsion Joint Specialist*, 1972.

[29] D.L. Huff. *Noise Reduction Technologies for Turbofan Engines*. Glenn Research Center, Cleveland, Ohio, 2007.

[30] Hunter C. Massey S. Mengle V.G. Pao P. Thomas R. Elmiligui, A. *Computational Analysis of a Chevron Nozzle Uniquely Tailored for Propulsion Airframe Aeroacoustics*. 27th AIAA Aeroacoustics Conference, 2006.

[31] A. Linke-Dieslinger. *Systems of Commercial Turbofan Engines*. Springer, Berlin, Heidelberg, 2008.

[32] 14 CFR § 33.77 Foreign object ingestion ice., 2014.

[33] 14 CFR § 33.17 Fire protection., 2014.

[34] T. Bingelis. *Firewalls*. Experimenter, 1995.

[35] D Jung. K Lee S. Cha. J, Choi. and B Hunter. *"Advanced Emergency Power System Using Thermal Battery for Future Aircraft"*, volume San Diego, California, AIAA 2006-4161. 4th International Energy Conversion Engineering Conference and Exhibit (IECEC), 2006.

[36] Kendell R. Full authority digital control for civil aircraft engines. *The American Society of Mechanical Engineers*, 1981.

[37] Bosco C.J. Lenox T.G. Barley, B.A. Full authority digital electronic control highlights of next generation propulsion control technology. *The American Society of Mechanical Engineers*, 1978.

[38] 14 CFR § 33.67 Fuel system., 2014.

[39] 14 CFR § 33.71 Lubrication system., 2014.

[40] Carr D. Dong J., Migdal C.A. *Aircraft Engine Lubricants*. Wang Q.J., Chung YW. (eds) Encyclopedia of Tribology. Springer, Boston, MA., 2013.

[41] Garfinkle J.B. Marks K.E. Birkler, J.L. Development and production cost estimating relationships for aircraft turbine engines. Technical report, Rand, 1982.

[42] Eia-u.s. kerosene-type jet fuel wholesale per resale price by refiners, 2020.

[43] R.J. Morrison J Bonnefoy P., Hansman. Investigation of the impacts of effective fuel cost increase on the us air transportation network and fleet. 10th AIAA Aviation Technology, Integration, and Operations Conference., sep 2010.

[44] Al-Shamma O. Ali, R. A comparative study of cost estimation models used for preliminary aircraft design. *Global Journal of Researches in Engineering: B Automotive Engineering*, 14, 2014.